AD-A121 321 COMPARISON OF RAMAN SCATTERING METHODS FOR COMBUSTION DYNAMICS MEASUREMENTS(U) GENERAL ELECTRIC CORPORATE RESEARCH AND DEVELOPMENT SCHENECTADY NY M LAPP ET AL. 1/1

UNCLASSIFIED OCT 82 AFOSR-TR-82-0969 F/G 7/4 NL

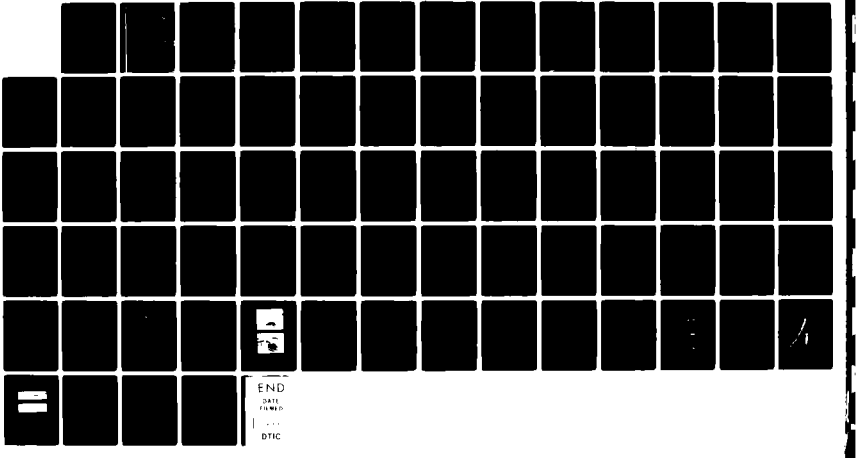

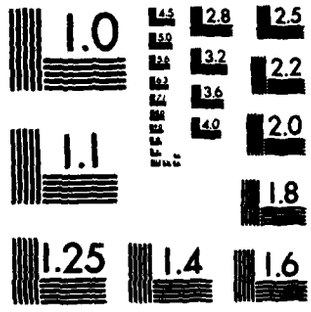

AFOSR-TR- 82-0969

COMPARISON OF RAMAN SCATTERING METHODS FOR COMBUSTION DYNAMICS MEASUREMENTS

Final Scientific Report

May 1, 1977 through January 30, 1981
Contract F49620-77-C-0094

Submitted to

DIRECTORATE OF AEROSPACE SCIENCES
AIR FORCE OFFICE OF SCIENTIFIC RESEARCH
BOLLING AIR FORCE BASE, DC 20332

October, 1982

APPROVED FOR PUBLIC RELEASE: DISTRIBUTION UNLIMITED

Prepared by

General Electric Company
Corporate Research and Development
Schenectady, New York 12301

UNCLASSIFIED

SECURITY CLASSIFICATION OF THIS PAGE (When Data Entered)

REPORT DOCUMENTATION PAGE		READ INSTRUCTIONS BEFORE COMPLETING FORM
1. REPORT NUMBER AFOSR-TR- 82-0969	2. GOVT ACCESSION NO. A121321	3. RECIPIENT'S CATALOG NUMBER
4. TITLE (and Subtitle) COMPARISON OF RAMAN SCATTERING METHODS FOR COMBUSTION DYNAMICS MEASUREMENTS		5. TYPE OF REPORT & PERIOD COVERED FINAL REPORT 01 May 77 - 30 Jan 81 6. PERFORMING ORG. REPORT NUMBER
7. AUTHOR(s) M LAPP, MC DRAKE, CM PENNEY, and S WARSHAW		8. CONTRACT OR GRANT NUMBER(s) F49620-77-C-0094
9. PERFORMING ORGANIZATION NAME AND ADDRESS GENERAL ELECTRIC CO. CORPORATE RESEARCH & DEVELOPMENT P.O. BOX 8, SCHENECTADY, NY 12301		10. PROGRAM ELEMENT, PROJECT, TASK AREA & WORK UNIT NUMBERS 61102F 2308 A1
11. CONTROLLING OFFICE NAME AND ADDRESS AIR FORCE OFFICE OF SCIENTIFIC RESEARCH/NA BOLLING AFB, DC 20332		12. REPORT DATE October 1982 13. NUMBER OF PAGES 72
14. MONITORING AGENCY NAME & ADDRESS(if different from Controlling Office)		15. SECURITY CLASS. (of this report) UNCLASSIFIED 15a. DECLASSIFICATION/DOWNGRADING SCHEDULE

16. DISTRIBUTION STATEMENT (of this Report)

APPROVED FOR PUBLIC RELEASE; DISTRIBUTION UNLIMITED.

17. DISTRIBUTION STATEMENT (of the abstract entered in Block 20, if different from Report)

18. SUPPLEMENTARY NOTES

19. KEY WORDS (Continue on reverse side if necessary and identify by block number)

COMBUSTION
OPTICAL DIAGNOSTICS
TEMPERATURE
DENSITY
COMPOSITION
RAMAN SCATTERING
CARS (COHERENT ANTI-STOKES RAMAN SPECTROSCOPY)
PARTICLE LUMINOSITY
SOOT

20. ABSTRACT (Continue on reverse side if necessary and identify by block number)

Light scattering optical probes can provide spatially- and temporally-resolved measurements of temperature and molecular composition without appreciably perturbing the combustion process. The zones of applicability for pulsed vibrational Raman scattering (VRS) in combustion have been explored through experimental studies of laminar premixed and turbulent diffusion flames with various gaseous fuels. The relative applicabilities of VRS and

DD FORM 1 JAN 73 1473 EDITION OF 1 NOV 65 IS OBSOLETE

UNCLASSIFIED

SECURITY CLASSIFICATION OF THIS PAGE (When Data Entered)

CARS (coherent anti-Stokes Raman spectroscopy) to simple flames and practical combustion devices are discussed. Major limitations of VRS (and, to a lesser extent, CARS) are identified as laser-induced particle incandescence and molecular fluorescence. Analyses of these problems are given as well as suggestions for minimizing their effects.

CONTENTS

COMPARISON OF RAMAN SCATTERING METHODS FOR COMBUSTION DYNAMICS MEASUREMENTS

OBJECTIVE

Light scattering optical probes for combustion research have received strong attention lately because of their ability to provide simultaneous spatially- and temporally-resolved measurements of temperature and molecular composition without appreciably perturbing the combustion process.

In this work, our objectives were (1) to explore the zones of applicability of pulsed vibrational Raman scattering (VRS) for combustion measurements through experimental studies of laminar premixed and turbulent diffusion flames with various gaseous fuels, and (2) to compare the relative applicabilities of VRS and coherent anti-Stokes Raman spectroscopy (CARS) to simple flames and practical combustor devices.

The major limitations of pulsed Raman scattering (and, to a lesser extent, CARS) identified in the experimental program were laser-induced particle incandescence and molecular fluorescence. Analytical analyses of these problems are treated in detail and some suggestions for minimizing them are given.

I. EXPERIMENTAL RAMAN AND COMBUSTION APPARATUS

A. Laser Raman Apparatus

A schematic overview of the combustor geometry optical configuration and electronic data processing used in this work is given in Figure 1. [1] A horizontally burning flame - either a laminar premixed flame from a porous plug burner or a turbulent diffusion flame from the turbulent combustor - is positioned for study relative to a fixed-bed Raman optic configuration. The laser used to excite the Raman scattering is a Candela dye laser, which consists of an oscillator and two amplifiers pumped by linear flashlamps. The oscillator output is tuned and line-narrowed by three intracavity prisms placed just before the totally reflecting mirror. The amplified output is deflected through 180° by three additional prisms, and directed along a 3-m path to a 1.5-cm aperture which spatially and spectrally filters the laser beam. This configuration ensures a sharp focus and removes unwanted background light from flash lamps and dye fluorescence. The laser beam is focused by a 200-mm focal length lens into a small region of the flame. The laser power for each laser pulse is measured by a vacuum photodiode while the approximate spectral distribution of each laser pulse is monitored by a 1/4-m Littrow-mount grating spectrometer with TV camera readout. The laser produces pulses of about 1 J at the test zone, within a 0.2-nm bandwidth tuned to 488 nm. The pulse duration is 1-2 μs, and a repetition rate up to 1 pps is obtainable with these output parameters.

Light scattered at right angles from the incident laser beam is collected by two lenses and focused through the entrance slit of a Spex 3/4-m single spectrometer. The laser focus and collection optics magnification gives a sample volume (spatial resolution) of 0.3 x 0.3 x 0.7 mm (greatly exaggerated in Figure 1). At the exit plane of this spectrometer, five photomultiplier tubes (PMT's) detect anti-Stokes vibrational Raman scattering from N_2 and Stokes scattering from N_2, O_2, H_2 and H_2O. Signals from the photomultipliers and laser detector are sampled several microseconds before and after the laser pulse. Both the 'before' and 'after' signals from each detector are digitized and their difference represents the net Raman signal. Temperature is determined by the intensity ratio of anti-Stokes to Stokes N_2 VRS signals and the concentrations of N_2, O_2, and H_2O are determined by the intensities of their respective Stokes signals normalized by the laser energy. Corrections are made for photomultiplier sensitivities, Raman cross sections, and Raman band contour temperature variations. A fifth photomultiplier detector located at the side-port exit slit of the Spex monochromator monitors pulsed Rayleight scattering.

The data collection is controlled by a microcomputer which fires the laser, collects and digitizes the signals from the energy meter and PMT's, and stores the data on floppy disc or cassette tapes for subsequent processing. Steps in signal processing are shown on the bottom of Figure 1. Scattering intensities for N_2 anti-Stokes and N_2 Stokes signals are measured for each laser pulse. Their ratio can be related to values of temperature based upon theoretical calculations and calibrations. Repetitively pulsing the laser at the same flame location

permits the buildup of a probability density function (pdf) for temperature. Similarly, molecular concentrations of H_2, N_2, H_2O and O_2 are determined from every laser shot from the corresponding Stokes scattering intensity normalized by laser energy, and pdf's of these scalars are built up in the same way. As in temperature measurements, corrections are made for photomultiplier sensitivities, Raman cross sections, and Raman band contour variations with temperature.

B. Laminar Premixed Flames

The goals of this work have included diagnostics of both laminar premixed and turbulent diffusion flames, in order to study Raman scattering measurement limitations under limiting conditions. The laminar premixed flames studied here were produced on a water-cooled porous plug burner (diameter 2.5 cm) burning into another water-cooled porous plug (of larger diameter) placed 2.0 cm away and connected to a rough vacuum line. In this way, a stable, horizontally burning flame at atmospheric pressure was produced which had the advantage of uniform flame conditions for the test zone defined by the intersection of the vertically-passing laser beam with the collection optical path.

Accurate flow metering techniques (using critical flow through orifices monitored by precision pressure gauges) were utilized to produce reproducible and clearly-defined flame conditions. The critical flow orifices were calibrated in our laboratory through the use of basic volume displacement techniques.

In the next section, the turbulent diffusion flame test facility is described. The entire porous plug assembly just described can be fit inside the test zone of this turbulent combustor by removing one of its windows, so that the optical paths for the laminar premixed and turbulent diffusion flames could be made essentially identical for the purposes of system calibration.

C. Turbulent Combustor Facility

Turbulent diffusion flames were produced for this work in a jet diffusion flame combustor, constructed with a view toward flexible use for fundamental turbulent combustion studies. Although the basic flow-induced tunnel design could accommodate, in principle, a variety of combustor configurations (i.e., jet diffusion, rearward facing step, splitter plate, bluff body, swirl, etc.), a turbulent jet diffusion flame (a central jet of fuel surrounded by a coflowing air stream) was chosen for this study for the following reasons:

1) Turbulent jet diffusion flames provide reproducible and easily characterized fuel-air mixing in the shear layer between the two gas streams.

2) They permit easy control of turbulence mixing levels by variation of the initial velocities of each stream.

3) They have been studied extensively (at least for H_2-air systems) by physical probe techniques by Bilger and others. [1]

4) They permit simplification of theoretical modeling approaches, in order to consider more clearly their key elements.

5) They are easily duplicated (because of the simplicity of design) in other laboratories for verification of experimental results and evaluation of new experimental techniques.

Figure 2 contains a diagram of the combustor. A 7 h.p. fan with a maximum rated throughput of 1450 cfm (Barry Industrial Fan, Model 609-DT) mounted on the roof of the laboratory draws conditioned room air into the combustor tunnel. The tunnel was designed to minimize background air flow turbulence levels in the test section through the use of an inlet section containing a large, square 0.56 cm x 0.56 cm bellmouth, a honeycomb flow straightener, 5 screens, and a 14-to-1 area contraction section. Additionally, provisions have been made to inject 1-μ diameter alumina seed particles into the air and/or fuel flow for laser velocimetry measurements.

The inlet section is attached by a flange to the 0.15-m square by a 2-m long test section which has large flat pyrex windows on all four sides, providing excellent optical access to the flame for a length of 0.89 m. Because these windows are epoxied to aluminum frames which attach to the test section by O-ring seals, each window is easily demounted for cleaning or for insertion of metal sideplates containing physical probes or special windows. (See, for example, Figure 3.)

Hot-film anemometers, pitot static probes and pressure taps in the metal sidewall shown in Figure 3 were used to check the quality of the air flow in the combustor. For example, the rms turbulence levels in the test zone, sensed by hot-film anemometry, were found to be 0.2% at a flow velocity of 10 m/s. Low background turbulence in the initial air flow is important to insure that the fuel/air mixing is induced predominantly by the shear-induced turbulence in the mixing layer between the two flows.

The central fuel tube (3.2-mm internal diameter and 1.6-mm wall thickness with an external taper over a 2-cm length to a knife-edge tip) is centered in the entrance of the test section by metal struts near the combustor inlet and fine wire spiders near the fuel tube exit. The fuel flow rate is controlled by the same critical flow metering techniques as are used for the porous plug burners. Air velocity in the test section is servo-controlled over the range 1 to 30 m/s. the fuel-to-air velocity ratio is, typically, varied from 2 to 10, producing H_2-air turbulent diffusion flames whose lengths range from 50 cm to greater than 1 m.

The 0.15-m square test section slides into a larger 0.18-m exhaust duct with tapered Teflon wedges to give a more gradual transition. The exhaust ductwork is designed with two stainless steel honeycomb sections, aerodynamically designed turning vanes at all corners, and rubber gaskets to prevent flow disturbances or fan-induced vibrations from propagating back into the test section.

The purpose of this sliding fit at the end of the test section as well as the flexible rubber section in the exhaust ductwork is to make

the inlet and test sections movable in three dimensions (see Figure 2b) in order to permit flame profile studies using fixed-bed optical probes. Positioning accuracy (within a fraction of a mm) for the movable combustor is obtained by precision screw drives. This combustor design thus facilitates maintenance of the demanding optical alignments required in tests of optical diagnostics such as have been carried out here, and becomes particularly useful for work carried out with the facility that involves the coupling together of separate optical probes (such as, for example, pulsed Raman scattering and laser velocimetry).

II. RESULTS OF RAMAN SCATTERING FROM LAMINAR PREMIXED FLAMES

A. Calibrations

The Raman detection system described in Section I.A. must be calibrated in order to provide accurate measures of temperature and molecular density. This calibratio was carried out in two independent ways. First, a standard lamp with known intensity as a function of wavelength was used to measure the relative sectral response of the spectrometer and the various photomultipliers at each of the detected wavelength regions. Then signals from the individual Raman channels were corrected for the measured spectral response of the spectrometer-PMT system, the relative Raman cross sections of the different molecules, and the temperature-dependent fractions of the calculated vibrational Raman bands which fell within the experimentally determined spectral bandpasses. (This form of calibration can be used in an absolute sense, or in a hybrid fashion, relative to a room temperature nitrogen measurement, in order to calculate various flame species densities and temperatures from measured Raman signals.)

The second independent procedure utilizes Raman measurements of ambient air and room temperature H_2 to determine Raman intensities of known molecular gas densities. Calibration of the relative sensitivities of N_2 vibrational Stokes and anti-Stokes channels for temperature measurements was made by comparison of temperatures measured by pulsed Raman techniques with those previously determined in isothermal laminar, premixed H_2-air flames by radiation-corrected fine-wire thermocouples and by cw VRS bandshape analysis. [3] The flame temperatures for this burner are far below calculated adiabatic flame temperatures for the H_2-air mixtures utilized because of appreciable heat losses to the water cooled porous plug. Similarly the calibration factor for H_2O vapor was determined from Raman measurements of laminar, premixed H_2-air flames where the N_2-to-H_2O mole fraction ratios could be calculated from known input gas compositions. The calibration is extended to other temperatures, as in the lamp calibration just described, by using calculations of the fraction of the vibrational Raman band which falls within the measured experimental bandpass. (Water vapor measurements are somewhat less certain because calculations at high temperatures of water bandshapes are of limited accuracy in the 'tail' of the contour. This part of the VRS contour is increasingly important at elevated temperatures, and is uncertain because of insufficient knowledge of the energy level structure of water vapor - especially, the rotational structure of excited vibrational levels.)

In practice, the standard lamp calibration was performed once, and the laminar flame calibration measured every few days, while N_2 room temperature calibrations are checked several times each day. Close agreement with room air shots for the nitrogen Stokes channel, and with lamp calibrations for all channels, is taken to indicate satisfactory system alignment and performance.

Experimental pulsed Raman measurements (from 200 laser-shot runs) of temperature and major species mole fractions for two such laminar, premixed H_2-air flames (ϕ = 1.0 and 0.55) are compared in Table 1 with the theoretical burnt gas mole fractions calculated from the initial

compositions and the temperature measured previously by fine-wire thermocouples and cw Raman bandpass analysis. The agreement is excellent, indicating that systematic errors are acceptably low (∿40K for temerature and 1 percent for mole fraction of major species for the range of premixed flames studied.)

B. H_2-Air Flames

In addition to system calibrations, analyses of Raman scattering from laminar, premixed H_2-air flames help define our measurement resolutions under the best possible combustion conditions for Raman measurements -- very small fluctuations from any remnant turbulence, and low background luminosity. For example, Figure 4 shows the temperature pdf from a 200 laser-shot data set obtained from an essentially isothermal zone (whose temperature was known from previous calibrations) in a premixed stoichiometric H_2-air flame. [1] We expect this pdf to be a sharply-peaked function. Since the widths of such measured distributions are caused primarily by measurement uncertainties, they define our experimental resolution for the Raman technique described here. Repeated determinations of the temperature pdf for this flame are characterized by a symmetric distribution about an average temperature of 1550 K. Table 1 includes a more detailed analysis of pulsed Raman measurements of two different H_2-air premixed flames giving average values, relative standard deviations, and normalized moments of the pdf distributions for temperature and mole fractions of all the major flame species. [1] In both flames, temperature pdf's are characterized by a 4% relative standard deviation.

In order to determine whether or not the relative standard deviations found from calibration pdf's of the type shown in Figure 4 were reasonable, theoretical estimates of precision were first made using a propagation-of-errors analysis. The relative standard deviation, RSD, for an individual temperature measurement (single laser shot) can be calculated approximately from

$$RSD_T \simeq \frac{1}{T}\left[\left(\frac{\partial T}{\partial N_S}\sigma_S\right)^2 + \left(\frac{\partial T}{\partial N_{AS}}\sigma_{AS}\right)^2\right]^{1/2} \qquad (1)$$

where $\sigma_S = \sqrt{\bar{N}_S}$ and $\sigma_{AS} = \sqrt{\bar{N}_{AS}}$ are the standard deviations in the individual photon counts. Here $\bar{N}_S$ and $\bar{N}_{AS}$ are average values of detected photon numbers for N_2 Stokes and anti-Stokes vibrational Raman scattering, respectively. The approximation is good if $\sigma_{AS}/\bar{N}_S$ and σ_{AS}/N_{AS} are small compared to unity. This can be simplified to

$$RSD_T \simeq \frac{T}{\theta_V}\left[\frac{1}{\bar{N}_S} + \frac{1}{\bar{N}_{AS}}\right]^{1/2} \qquad (2)$$

where θ_V for N_2 equals 3374K. Here, the characteristic temperature, θ_V, corresponds to the population of the first excited vibrational level for a particular molecular species (in this case, N_2) being (1/e) times the

total population for thermal equilibrium conditions. The number of photons detected in each channel can be determined either by experimental measurement or by calculations which include known laser intensity, Raman cross section, collection efficiency, and detector quantum efficiency. Either method gives approximately the same result. As an example, with an incident laser pulse of 1 J, $\bar{N}_{AS} = 128$ and $\bar{N}_S = 1265$ detected photons for scattering from N_2 in a H_2-air flame at 1500 K. Values corresponding to other temperatures can be calculated from the known dependence on temperature of the Stokes and anti-Stokes intensities. Using these values we have calculated the relative standard deviation as a function of temperature and N_2 density for our experimental configuration, with the result that the RSD for temperature will remain nearly 4% for all expected stoichiometries and temperatures, except for rich mixtures below 950 K where they are larger. The very good agreement between theoretical predictions for the RSD for temperature (4%) and the experimental results in Table 1 suggest that the spread in the pdf shown in Figure 4 can be almost entirely ascribed to the expected statistical fluctuations in the number of detected photons per laser shot.

Similar calculations for the expected RSD single shot measurements of species concentration or mole fraction measurement indicate

$$RSD_S \approx \frac{\sqrt{\bar{N}_S}}{\bar{N}_S} \qquad (3)$$

which for N_2 at 1500 K equals 3%. However, the standard deviation in concentration is also increased by temperature uncertainties which affect concentrations through the correction factor for the fraction of the Raman and in the experimental bandpass. For N_2 at 1500 K a 4% temperature fluctuation increases the standard deviation in N_2 concentration by 0.8% for a total $\sigma \approx 4\%$. This agrees with the measured standard deviation of 4% for N_2 in Table 1.

Relative standard deviations for concentrations of other molecular species can be calculated from Eq. (3) by determining the Stokes vibrational Raman signal obtained from that molecular species (proportional to the molecular concentration, the relative sensitivity of that PMT channel, and the fraction of the total Raman band collected). For the same 1500 K flame, the calculated RSD values (including the effects of a 4% temperature fluctuation) are 6% and 11% for H_2 and O_2, respectively, compared with the measured values of 9% and 15%. Thus, the measured values of molecular concentration fluctuations for steady, laminar flames are also substantially controlled by photon counting statistical fluctuations.

C. Propane-Air Flames

In an effort to assess the feasibility of extending pulsed Raman measurements to hydrocarbon flames, several propane-air and H_2-propane-air premixed, laminar flames were investigated. No experimental difficulties were encountered in nonsooty burnt gas regions of these flames. For example, in a propane-air flame of fuel/air

equivalence ratio, ϕ, equal to 1.5, for which the gas flow velocity was set nearly equal to the burning velocity (18 cm/s) to minimize heat losses to the burner, the measured average temperature from pulsed Raman scattering in the burnt gas flame region 1 cm from the burner was 2048 K, with a relative standard deviation of 5%. This temperature is close to the calculated adiabatic temperature of 1971 K. Flames of other equivalence ratios and flow rates also gave measurements in agreement with calculated values when reasonable heat losses to the burner were included. Thus, the agreement within experimental error between the measured and calculated temperatures and the low measured standard deviation of 5% strongly indicate that the increased luminosity of propane-air flames has no deleterious effect on our pulsed Raman measurements. This result is expected because the 'before' and 'after' sample-and-hold electronics subtracts out most of the luminous flame backgrounds from each Raman channel.

However, great difficulty was found in making meaningful Raman measurements in sooty regions of very fuel-rich ($\phi \geq 3.0$) propane-air premixed flames because of large laser-induced backgrounds. Background interferences caused by soot or soot precursors are well illustrated by measurements obtained from an intermittently sooting region in rich premixed propane-air flames ($\phi = 3$) produced on the porous plug burner. These flames were observed on the burner axis at a point 3 mm above the flame front, where, in the rich flame, the orange glow characteristic of soot thermal emission was just becoming well established. A slight flickering of this region was visible to the eye, and photomultiplier observation showed it to be clearly oscillatory. Background interference in pulsed Raman measurements was evaluated by slowly sweeping the spectrometer drive as the laser fired continuously at $\sim$1 pps. In a gas region free of background interference, this procedure traces out a slit function convoluted with the Raman line shape for each Raman channel, such as the result shown at the toip of Figure 5 for N_2 in the stoichiometric flame. [4,5]

In the rich flame, frequent off-scale readings were obtained, as shown in the middle plot in Figure 5, although the pre-pulse levels were always well on scale. Thus the off scale readings were caused by a laser-induced signal rather than the natural luminosity of the flame. However, an appreciable fraction of the laser shots produced data which were on-scale in all channels. Just this data was used by means of conditioned sampling on the bottom plot in Figure 5, illustrating that a reasonable reproduction of the slit function can be obtained from the on-scale data. We conclude that the sooting region was oscillating in and out of the Raman measurement volume.

Thus, it appears that pulsed Raman measurements can be obtained in some intermittently sooting or otherwise strongly luminous regions at times when the soot or other luminous source density is very low. Generally, however, straightforward Raman measurements will be obscured by laser-induced background in regions where the soot or other laser-induced luminous source densities are large. Potential sources for this background include laser-induced particle incandescence or molecular fluorescence. Since these processes appear to be the major limiting factors for single-pulse spontaneous Raman measurements in gaseous hydrocarbon flames, they are examined in detail in Section IV.

III. RESULTS OF RAMAN SCATTERING FROM TURBULENT FLAMES

A. Raman Measurements on H_2-Air Flames

Meaningful measurements on turbulent flames require techniques that have sufficient temporal and spatial resolution to make statistically significant measurements on homogeneous sample volumes within the flame. Work in this laboratory (funded in part by this AFOSR contract and also by General Electric, ONR and DoE) has demonstrated that pulsed Raman scattering is a reliable, quantitative technique for spatially and temporally resolving simultaneous measurements of temperature and concentrations of all major molecular species in turbulent H_2-air diffusion flames. Extensive data have been taken and results are presented in the form of average values, scalar pdf's and their normalized moments, and comparison plots of species concentration vs. temperature. Comparison with adiabatic flame calculations -- quantitatively including the effects of radiative heat loss and incomplete combustion -- demonstrates that differential molecular diffusion (i.e., *preferential* diffusion of H_2) is an important process in fuel-rich flame regions of moderate Reynolds number (i.e., Re=1500 flames).

These results are presented here to demonstrate the accuracy of the pulsed Raman technique in turbulent flames - a goal of this AFOSR effort - and, additionally, as an example of the application of this data to develop insights into important flame processes and the validities of modeling assumptions.

Two different H_2-air turbulent jet diffusion flames in the turbulent combustor described in Section I have been extensively investigated. Flame 1 had an initial H_2 average velocity at the fuel tip of 50 m/s (calculated *from previously* calibrated volumetric flows and the known fuel tube cross-section), corresponding to a Reynolds number of 1500, based upon the H_2 cold flow through the 3.2-mm-i.d. fuel tube. An air flow of 10 m/s (measured by pitot tube and hot film anemometry) surrounded the fuel tip for an initial H_2-to-air speed ratio of 5. The visible flame was $\sim$1 m in length with a maximum diameter of $\sim$25 mm and a maximum rise due to buoyancy of $\sim$10 mm at the flame tip. The second hydrogen-air turbulent flame studied (Flame 2) had initial velocities of H_2 and air of 150 m/s and 15 m/s, respectively. The Reynolds number of the jet was therefore increased to 4500 while the initial H_2-to-air speed ratio increased to 10. As expected, the appearance of the flame was markedly changed, with the visible flame length decreasing to $\sim$0.9 m, and flame fluctuations increasing significantly.

Figure 6 shows probability density functions (pdf's) for temperatures measured in three different H_2-air flames with our pulsed Raman apparatus. [1] The pdf to the left in Figure 6 shows the temperature histogram from a 200 laser shot data run obtained from an essentially isothermal zone (whose temperature was known from previous calibrations) in a premixed stoichiometric H_2-air flame. We expect this pdf to be a sharply-peaked function, and the width of the measured distributions defines our experimental resolution for the Raman technique described here. Measurement resolution is discussed in detail in Section II, but the pdf is repeated here for comparison with the two

pdf's measured in turbulent flames. The pdf's at the center and right-hand sides of Figure 6 were obtained in the experimentally-determined mixing layers of Flame 1 and Flame 2, respectively, and represent the broadest pdf's observed in these flames at an axial location of 50 diameters downstream of the fuel nozzle. The much wider distribution of the pdf's in the turbulent flame are the result of real temperature fluctuations in the flame. Note that the center pdf in Figure 6 shows no signs of intermittency (i.e., no evidence of a bimodal pdf shape) in agreement with the steady appearance of this flame. The pdf to the right in Figure 6 has a much broader distribution (from room temperature to the adiabatic H_2-air flame temperature) and does display pronounced intermittency which reflects the change in flame character caused by the increase in turbulence level in Flame 2.

Table 2 shows average values, standard deviations and normalized zero moments calculated from the temperature pdf's of Figure 6. The normalized zero moments (denoted Z_L) in Table 2 are calculated by

$$Z_L = (\bar{x})^{-L} (J)^{-1} \sum_{j=1}^{J} (x_j)^L \qquad (4)$$

where $\bar{x}$ is the average value and x_j the instantaneous value of the variable summed over the number of data points J in the sample. The value of Z_1 is, by definition, equal to 1. If all of the values of x_j are identical, i.e., if the measured property is a constant, then all of the moments $Z_L = 1$. However, as the distribution of x broadens, the higher moments (Z_L for $L > 1$) will increase. These zero moments can be converted easily to central moments such as mean square deviation, skewness, and kurtosis.

The pdf's of concentration of H_2, N_2, O_2 and H_2O show similar effects as in Figure 6. Table 3 summarizes Raman results obtained at the centerline and mixing layer of both the Re = 1500 and 4500 turbulent diffusion flames as well as for the laminar premixed flame. The relative standard deviations of each scalar variable measured in the turbulent flames have larger values in the mixing layer compared to the centerline, and larger values for the Re = 4500 flame than the Re = 1500 flame, indicative of the relatively higher levels of turbulent fluctuations present under these respective conditions.

Extensive Raman data were taken in Flame 1 at five downstream positions [x/d = 25-150 were x is the axial (horizontal in this horizontally burning flame) distance measured from the fuel tip]. At each value of x/d, data were taken at various off axis positions, y/d = -7 to +7, where y is the vertical distance from the extension of the fuel tube centerline to the measurement zone. Typically 200 laser shots (data points) were taken at each flame location studied. To illustrate these results, radial profiles of average values of molecular concentrations have been calculated from the pdf data. [1] For example, Figure 7 presents average values of mole fractions of the major flame species at an axial location of x/d = 25. These transverse profiles show, as expected, high H_2 concentrations in the center which decrease going to the edge of the flame, and the opposite trends for N_2, H_2O, and

O_2.

Further downstream, these profiles change. Figure 8 presents results at x/d = 100. The H_2 mole fraction decreases and the various mole fraction profiles tend to flatten out.

In the data presented in Figures 7 and 8 the O_2 mole fraction was not measured directly, but was calculated assuming that the overall ratio of nitrogen atoms to oxygen atoms remained a constant in all parts of the flame. Subsequent data wherein the O_2 concentration was measured directly has shown the same behavior. Additionally, the temperature profiles also flatten appreciably as x/d increases, as can be seen in Figure 9, where results are plotted for x/d = 25, 100, and 150. Asymmetry is clearly visible in Figs. 7, 8, and 9, the center of the temperature or molecular species profiles rises $\sim$8 mm from the projected fuel tube centerline at x/d = 150, as a result of buoyancy on this horizontally burning flame. These average value plots show trends qualitatively similar to Kent and Bilger's data [2] on similar flames using physical probe techniques.

The key point in the work presented here is that, in addition to average values, the pulsed Raman data from our experiments give a direct measure of the fluctuations about these average values. Data presented in the form of individual pdf's or their calculated moments are useful because theoretical models are being developed based upon these functions as inputs. However, this type of presentation does not fully utilize the information in these Raman measurements, because it does not take into account the simultaneous nature of the temperature and concentration measurements. This aspect of the data can be represented in the form of three-dimensional joint pdf plots, which show the probability for obtaining simultaneous values of two variables. Alternatively, plots could show the distribution of a function of simultaneous values (for example the product of hydrogen and square root of oxygen densities) which may be useful in characterizing finite rate chemistry effects. Other data analysis techniques (i.e., mixture fraction-conditioned averages) which may be more sensitive indicators of finite rate chemistry are also being explored.

We have found that scattergrams of simultaneous measurements of two quantities are perhaps the most useful presentations for comparison of data to model predictions. In this form, the density of points on the scattergram takes the place of the third dimension in a three-dimensional joint pdf plot. We have called these scattergrams 'comparison plots' because they facilitate a direct comparison with several different flame models. The comparison plot presentations are discussed in the following section on Comparison with Theories.

B. Comparison with Theories

In other sections of this report we describe the overall experimental aspects of our light scattering/combustion measurement program. Here we point to new results obtained in that effort (on the differential diffusion of H_2 fuel) -- as an illustration of an investigation into basic flame processes, which makes available additional information concerning the fundamental assumptions used in

flame modeling. The canonical type of experiment described for our turbulent combustion program is well-suited for this kind of investigation, since it can, to a substantial extent, isolate key features of a combustion process, and thereby bring to bear relatively clear evidence about one's ideas concerning this process.

In order to develop advanced flame models, new information concerning key flame processes is clearly required. We have already mentioned molecular diffusivity effects, many others also need strong clarification concerning their importance and magnitudes. One of the prime areas is that concerning the fundamentals of the processes controlling the chemical production term in advanced flame models. For example, the effects (or regimes where the effects can be neglected) of finite rate chemistry are of considerable importance not only in the implementation of modeling procedures, but in the very selection of the class of model to be adopted.

Figure 10 is a comparison plot of simultaneously acquired N_2 concentration vs. temperature data given by the points compared with a simple adiabatic equilibrium (AE) flame model represented by the solid line. [4] The AE calculations were performed for fuel/air equivalence ratios between 0.2 and 6 using the computer code of Gordon and McBride. [6] The initial conditions were fuel and air at atmospheric pressure (750 Torr) and temperature (298K). The air represented in these calculations included 1% by volume water vapor, representing a typical laboratory environment. According to the conservation equations, the AE model should describe the temperature and concentration fields accurately under the following assumptions:

(1) Radiation losses are negligible,

(2) Chemical reactions are effectively instantaneous (fast chemistry), and

(3) Mass and heat diffusion occur according to ideal assumptions (unity Lewis number, no differential diffusion).

The rough general agreement between experiment and theory in Figure 10 indicates that the adiabatic equilibrium model is a reasonable starting point for understanding H_2-air turbulent flames. However, slight deviations from theory are observed in lean (upper part of the curve) flame zones and more significant deviations are evident in rich regions. Similar plots have also been made for the concentrations of H_2 and H_2O versus temperature which give entirely compatible results -- large deviations in rich flame regions. Measured N_2 and H_2O concentrations were consistently higher than predicted by the AE model while H_2 concentrations were lower.

Several potential sources of systematic experimental errors were checked to see if they could explain the observed deviations. In particular, we found that the effect of possible concentration and temperature variations across the dimensions of the measurement zone (0.3 x 0.3 x 0.7 mm) could not account for the observed deviations and careful spectrometer recalibration and refinement of temperature-dependent corrections produced very small changes in the

data. Since our analysis of experimental errors could not account for the observed deviations, we examined the effects that would be caused by failure of each of the assumptions required to validate the AE model.

Radiative heat loss moves points of the nitrogen-temperature theoretical curve in Figure 10 in directions nearly parallel to the lean leg segment in the same temperature range. Thus, the effect of radiation losses is to shift the rich leg of the theoretical plot toward the experimental points without significantly altering the lean leg agreement. However, calculations of the maximum radiative heat loss that can be expected to occur over the time required for a gas volume to pass through the test zone (~0.1 s) show that the resulting changes in temperature (80K at 1800K) and concentrations are much too small to account for the observed deviations. For example, a radiative heat loss of ~250K is required to bring the theoretical curve into agreement with the rich leg experimental data ($x/d = 75$) at 1800K.

Finite rate chemistry is another potential cause of experimental deviations from the theoretical predictions. Qualitatively, the effect of incomplete combustion is similar to radiative heat loss. Also the effect should be greatest near the stoichiometric mixture fraction [7] (the high temperature 'nose' of the $C(N_2)$ vs. T plots). However, the large nonequilibrium effects required to bring the theoretical curves into agreement with experiment - particularly in very rich flame regions - and their consistent occurrences for every laser shot, do not appear compatible with the short (perhaps 0.1 ms) reaction time scales in hydrogen combustion.

Potential causes discussed above for the departure of experimental data from the AE model do not account for the observed deviations and, in particular, for the fact that the observed peak temperature at all axial positions is close to the adiabatic H_2-air flame temperature -- which would not be true if radiative losses or finite rates were the dominant effect. The explanation which emerges then is that the preferential diffusion of H_2 from rich flame zones, which can be characterized by a non-unit Lewis number, is the primary cause of the *observed experimental results.*

The effects of differential diffusion are anticipated to be greatest in laminar diffusion flames, steadily decreasing as the turbulence level increases and turbulent diffusion begins to predominate over molecular diffusion. Thus, we would expect the effect of differential diffusion in our mildly turbulent flame to be intermediate between that calculated recently for a laminar H_2-air diffusion flame by Miller and Kee [8] and the AE calculation. Our experimental results are in agreement with this expectation, i.e., the measurements of the concentration of N_2 versus temperature generally fall between these two theoretical curves, as illustrated in Figure 11. This strongly supports the conclusion that the deviations shown in the figure result primarily from differential diffusion -- a result that seems reasonable in light of the rapid diffusional capabilities of H_2 and the moderate turbulence level in this flame.

Recent calculations by R. Bilger [9] that include explicitly the effects of differential diffusion using perturbation techniques, are in

good agreement with our data. His results for the mildly turbulent flame described previously are shown superimposed on the data in Figure 12. Recent experiments performed on the more turbulent flame (Re=4500, hydrogen fuel tip velocity = 150 m/s, air velocity = 15 m/s) produced conditioned average results closer to the AE model, as expected from the reasoning above and as predicted by Bilger's calculations. Conditioned averaging was utilized in this case to separate lean and rich leg concentrations on the basis of hydrogen concentration.

These results help to establish the AE model as a useful first approximation for use in more detailed H_2-air models, and to define the range over which differential diffusion effects must be included. More importantly, however, the aspects of this work related to the limits of accuracy of scalar measurements using Raman techniques, have demonstrated that vibrational Raman scattering can produce

* A sufficient number of simultaneous scalar measurements (temperature and major flame species) to characterize a non-sooting turbulent diffusion flame well,

* with sufficiently high accuracy to make feasible relatively subtle comparisons of the physical phenomena contributing to the flame behavior (and of applicable models).

No other diagnostic method to date can produce such diversity of laboratory data with such high accuracy.

C. Measurement Difficulties in Hydrocarbon-Air Flames

Results from pulsed Raman scattering in premixed propane-air flames produced on porous plug burners (described in Section II.C) indicated that severe measurement difficulties would occur in sooty regions of hydrocarbon-air flames. To assess this problem in nonpremixed flames, a set of mesurements were made in propane-air and propane/H_2-air turbulent diffusion flames. These experiments were conducted in the same combustion tunnel used for the corresponding H_2-air flame studies.

Photographs of propane/H_2-air and H_2-air flames are shown in Figure 13, in order to facilitate discussion of the key results. The H_2-air flame indicated corresponds to Re=1500, and has been described in Section III.A. The propane/H_2-air flame, resulting from an initial fuel mixture of 10% propane and 90% hydrogen burning with the surrounding co-flowing air stream, exhibits a compound physical structure. Pulsed Raman data were taken throughout this flame, the results of which are summarized in Table 4 for the various spatial positions sampled.

Raman measurements were not successful at flame locations where yellow soot radiation was evident, or on the axial flame centerline before and after the bright luminous sooting zone. In these locations, all photomultiplier channels registered off-scale readings analogous to the results in fuel-rich premixed propane-air flames. (See Figure 5.) As was the case for the premixed flames, these offscale readings were the result of laser-induced soot incandescence or laser-induced broadband fluorescence, and not the result of ordinary flame luminosity. At other flame locations, reasonable results were obtained from the mean

values of pulsed Raman measurements of temperature and major species mole fractions.

In propane-air turbulent diffusion flames, the bright luminous zone included essentially all of the flame, and no successful Raman measurements were obtained. Thus, the results in hydrocarbon turbulent diffusion flames demonstrate the same measurement difficulties with pulsed Raman techniques as observed in sooty premixed hydrocarbon flames.

IV. THE LIMITATIONS OF LASER-INDUCED PARTICLE INCANDESCENCE AND MOLECULAR FLUORESCENCE IN RAMAN SCATTERING

The major limitation of pulsed Raman scattering identified in the experimental studies undertaken in this program is laser-induced background luminescence from sooty flame zones of hydrocarbon flames. Experiments on premixed, laminar flames and nonpremixed, turbulent flames indicate that meaningful pulsed Raman measurements are difficult to obtain in these regions because of high laser-induced background signals. Eckbreth[10] found that the focused high power (~10^8 to 10^{10} W/cm^2) laser beam required for such measurements strongly heats the soot particles. These hot particles create a laser-induced background of thermal radiation which can be stronger than intrinsic thermal radiation from the flame, and comparable to or stronger than typical Raman scattering signals. Also, thermal energy transferred from the soot particles to the gas, and additional chemical reactions caused by their suddenly increased temperature can seriously perturb the measured gas properties (e.g., N_2 vibrational temperature, major gas concentrations) if those properties have time to respond to this absorbed energy during the laser pulse.

A somewhat similar combination of background and perturbation problems can occur in regions where there is significant molecular absorption of the incident laser radiation (for example, from high molecular weight organic molecules known to occur in sooty flame regions). Here the interference can take the form of laser-induced fluorescence, while the fraction of absorbed laser energy which is not radiated can alter the measured gas properties.

Soot-induced and molecular absorption-induced problems in Raman scattering measurements have not been investigated over the full range of conditions likely to be encountered in combustion gases; however, individual observations, and analyses of these to be discussed subsequently, suggest that these problems will generally prevent straightforward applications of Raman scattering to sooty hydrocarbon flames. Possible solutions to these problems, which may allow Raman scattering measurements to be obtained in at least moderately sooting regions, will be described at the end of this section.

A. Absorption of Light Energy by Soot Particles

The focused laser beams used in single pulse Raman scattering (and CARS) have typical power densities on the order of 10^8 to 10^9 W/cm^2. Soot particles exposed to such light fluxes are heated at an extremely rapid rate, reaching their vaporization temperature (~4000K) in a small fraction of a nanosecond. The rate at which light energy is absorbed by a particle is given by

$$P_A = I_o \sigma_{ABS} \quad (1)$$

where I_o is the incident light power density and σ_{ABS} is the absorption cross section for the particle. For strongly absorbing, small (< 100 nm radius) spherical particles, the absorption cross section is nearly equal to the extinction cross section (scattering plus absorption) given by

$$\sigma_{EXT} = \frac{8\pi}{\lambda} \text{Im} \left[\frac{m^2 - 1}{m^2 + 2} \right] r^3 \qquad (2)$$

Here r is the particle radius, λ is the light wavelength, and m is the complex index of refractivity. The symbol Im denotes the imaginary part of the term in brackets. Although even small soot particles are not generally spherical, general conclusions drawn about them on the basis of this equation are likely to be at least qualitatively correct.

Values for the complex refractive index of soot in the literature range from $m = 2 - 0.3i$ to $m = 1.57 - 0.56i$, with the latter value preferred in recent work. These values substituted into Eq. (2) yield, respectively,

$$\sigma_{ABS} = 1.7 \cdot 10^5 \ (cm^{-1}) \ r^3 \qquad (3)$$

and

$$\sigma_{ABS} = 4.1 \cdot 10^5 \ (cm^{-1}) \ r^3 \qquad (4)$$

at 500 nm, in the middle of the visible range.

A useful alternative expression of the absorption cross section σ_{ABS} over a wider size range is

$$\sigma_{ABS} = \beta \pi r^3 / \delta \qquad r < \delta \qquad (5a)$$

$$\sigma_{ABS} = \beta \pi r^2 \qquad r > \delta \qquad (5b)$$

where δ is 100 nm and $\beta \cong 0.9$ is a correction for that part of the extinction due to scattering. This approximation applies also to particles larger than 100 nm and agrees well with Eq. (4) for the smaller particles.

B. Soot Characteristics

The characteristics of soot in hydrocarbon flames affect both the level of laser-induced background and the possibility of measurement perturbations. Although the actual properties depend strongly on the type of flame and position within the flame, it is possible to specify general ranges which characterize many combustion measurements. For example, the measured soot volume fraction in ethylene, benzene and pyridine flames (Haynes, et al.)[11] range from 10^{-9} to 2×10^{-6}, while number densities range from 10^{9} to 10^{12} per cm^3. Generally the largest number densities seem to correlate with low volume fractions, and thus very small particles, with diameters on the order of two or three nm. In laminar diffusion and premixed flames, where the time since the beginning of soot formation can be related to position in the flame, the mass average soot depends strongly on the rate of thermal (Brownian motion) coagulation, independent of the mode of soot formation. Analyses of this process[11] produce the size dependence shown as a function of volume fraction and time in Figure 14. The particle size estimate also allows rough estimates of soot number density and the consequent average separation between particles, as a function of time and volume fraction, also shown in Figure 14. The utility of these estimates is improved by their relatively weak dependence on the soot volume fraction. The moderate disagreement between the results shown in Figure 14 and the experimental results in mature soot regions is possibly explained by noting that the presence of turbulence tends to speed the rate of coagulation, producing larger particles. Furthermore, well downstream of the particle zone, larger particles seem to predominate, perhaps indicating that the smaller particles have disappeared through oxidation.

C. Rate of Particle Heating

The rate at which particles are heated by absorption of the laser radiation can be calculated neglecting cooling by conduction and radiation in these high fluxes. Thus

$$\frac{d\theta}{dt} = \frac{I_o \, \sigma_{ABS}}{C\rho \, (4\pi r^3/3)} = \frac{3 I_o \beta}{4 C \rho \delta} \left(\frac{\delta}{r}\right) \tag{6}$$

where C is the heat capacity and ρ is carbon density. Here the ratio (δ/r) is set equal to 1 if it is less than 1, from Eqs. (5a, 5b). Representative values at high temperatures are

$$C = 2.1 \ J/g^{\circ}K \tag{7a}$$

$$\rho = 2 g/cm^3 \tag{7b}$$

Note that in the particle size range up to 100 nm radius, the heating rate is independent of particle size. Thus, in a flux of $10^9 W/cm^2$, if we assume an initial temperature of 1500K, small soot particles will be heated to their vaporization temperature in

$$t_H \cong 0.1 \text{ ns} \tag{8}$$

while a 500 nm radius particle requires

$$t_H \cong 0.6 \text{ ns} \tag{9}$$

Even in such short times, it can be shown that the temperature nearly equilibrates throughout the particle.

D. Soot Evaporation Rates

Exposed to these high light fluxes, small-to-medium soot particles can effectively disappear by vaporization in a short fraction of a 1 μs Raman pulse (or even a 10 ns CARS pulse). The vaporization rate is determined by equating the energy absorption rate and energy consumption rate by vaporization. Thus for small particles

$$-L \frac{dM}{dt} = I_o \beta \pi \, r^3/\delta \tag{10}$$

where L is the heat of vaporization and M is particle mass. The kinetic energy of the vapor and energy taken up by additional heating (necessary to sustain the high rate of vaporization) are small (~ 10%) in comparison to the energy sink of vaporization. Differentiating

$$M = 4\pi \, \rho r^3/3 \tag{11}$$

with respect to time and substituting into Eq. (A10), we obtain, after integration

$$r = r_o \exp \left[-t/t_v\right] \tag{12}$$

where the characteristic time for vaporization is

$$t_v = \frac{4\rho_c L \delta}{I_o \beta} \tag{13}$$

Thus this time is independent of particle size for particles with radii smaller than 100 nm. There is some uncertainty about the appropriate

heat of vaporization, partly because it depends on the degree of polymerization of the resulting vapor. In the temperature range from 2000-4000K and high light flux levels, the predominant vapor constituent is likely to be C^3 and we shall use the thermal constants appropriate to this process; e.g.,

$$L = 7 \cdot 10^4 \text{ J/g} \tag{14}$$

In this case

$$t_v = \frac{6.2 \text{ J/cm}^2}{I_o} \tag{15}$$

Thus at an incident flux of 10^9 watts/cm^2, only about 6 ns is required to vaporize small soot particles to 1/e (37%) of their original radius, or 5% of their original mass. For large particles, the RHS of Eq. (10) is multiplied by δ/r. Accordingly, we obtain

$$\frac{dr}{dt} = - \frac{I_o \beta}{4L\rho_c} \tag{16}$$

In this case, the time required for nearly complete particle vaporization is

$$t_v = \frac{4L\rho_c r_o}{I_o \beta} = 60 \text{ nsec} \tag{17}$$

for an incident flux of 10^9 W/cm^2 and particle radius of 1 μm.

E. Peak Particle Temperatures

The thermal emission created by laser-heated particles depends strongly on the temperature they reach. Vaporization-controlled particle temperatures in the laser beam can be calculated using a method developed by Jones, Langmuir and Mackay[12]. The derivation assumes that the mass leaving the surface must equal that which would strike it per second in a vapor in equilibrium with the particle, given by

$$\frac{dM}{dt} = 4\pi r^2 p_v \left(\frac{M_v}{2\pi R\theta}\right)^{1/2} \tag{18}$$

where p_v is the vapor pressure, R is the universal gas constant and M_v

is the molecular weight of the vapor (~ 36). Thus in a vacuum, where no recondensation of carbon vapor occurs, the evaporation rate is given by Eq. (18). Vapor pressure is expressed by the Clausius-Clapeyron equation:

$$p_v = p_o \exp\left[\frac{L\,(\theta - \theta_o)}{R\theta\,\theta_o} M_c\right] \tag{19}$$

where M_c is the molecular weight of atomic carbon and p_o is the vapor pressure at a reference temperature θ_o. Substituting this value into Eq. (18), we find

$$I_o = \frac{4Lp_o}{\beta}\left(\frac{\delta}{r}\right)\left(\frac{M_v}{2\pi R\theta}\right)^{1/2} \exp\left[\frac{L\,(\theta - \theta_o)}{R\theta\,\theta_o} M_c\right] \tag{20}$$

where the factor (δ/r) is omitted from $r \Rightarrow 100$ nm in accordance with Eqs. (5a, 5b).

The relationship between peak particle temperature θ and light flux I_o from Eq. (20) is plotted in Figure 15 for $r = 10$ nm and $r \Rightarrow 100$ nm. We note that the temperatures shown for low fluxes can be less than the vaporization temperatures for carbon. The primary reason for this result is that the treatment assumes vaporization into a vacuum. Thus the temperatures it predicts are lower than would be expected in the present case, particularly for larger particles which will be surrounded by a high pressure vapor shell during the early stages of vaporization (see subsequent discussion). The trend toward higher temperatures is evident from the experimental data presented by Eckbreth[10]. His data show temperatures several hundred degrees higher than predicted by Eq. (20) at flux levels near 10^8 W/cm^2. It is likely that the difference between actual peak temperatures and predicted values will be much larger at higher flux levels.

F. Expansion of the Surrounding Vapor

If the particle vaporizes at the rate determined by its latent heat of vaporization, the volume V of surrounding vapor must expand at the rate

$$\frac{dV}{dt} = \frac{I_o \beta \pi r^2}{L\rho_v}\left(\frac{r}{\delta}\right) \tag{21}$$

where the factor (r/δ) is omitted for large particles ($R > 100$ nm), and ρ_v is the vapor density. Differentiating

$$V = \frac{4\pi}{3} (R^3 - r^3) \tag{22}$$

we obtain

$$\frac{dR}{dt} = \frac{I_o \beta r^2}{4R^2 L \rho_v} \left(\frac{r}{\delta}\right) \tag{23}$$

The density of C_3 vapor at 4500K and atmospheric pressure is 9.8×10^{-5} g/cm^2. If this value is substituted into Eq. (23), we find that the initial expansion rate of the vapor shell (that is, for r = R) for a 100 nm particle in a flux of 10^9 W/cm^2 is 3.3×10^7 cm/sec, or about 200 times the sound velocity! This result strongly suggests that the density and degree of polymerization of the carbon vapor must be much higher than assumed near the particle surface. It also raises the possibility that inertial and collisional confinement of the vapor may cause the particle to absorb much more energy than necessary for vaporization, thereby creating shock waves or ionization which could spread energy rapidly through the gas volume, causing measurement perturbations even on the time scale of nanoseconds.

G. Expansion Phenomena Versus Particle Size

Based on the previous discussion, we can speculate about the various processes which occur during vaporization of soot particles by an intense laser beam and how these processes depend on particle size. It will be assumed throughout this section that the laser flux rises instantaneously to 10^9 W/cm^2 and that it is uniform at this power density over the observed region.

i. Small Particles ($r \cong 5$ nm): The particle absorbs sufficient energy to vaporize in 6 ns. Although the initial molecule number density near the particle surface is very high, vaporization proceeds rapidly because the molecules are free to stream out to a distance of one mean free path in the combustion gases (~ 500 nm), requiring only about 0.3 ns to reach this distance at the average C^3 molecular velocity at 4500K. At this time, the average carbon molecule number density is low relative to the combustion gas density, on the order of or less than 1% of it, depending on the average molecular weight of the carbon molecules. For cases where the laser excitation wavelength does not correspond to absorption wavelengths of the carbon vapor molecules, absorption and consequent thermal or fluorescence emission of the carbon vapor derived from soot particles is likely to drop sharply after the particle is vaporized (i.e., within the first 10 ns of the pulse). However, effects of reaction of the vapor with surrounding combustion gases may sustain a higher level of fluorescence; this process is difficult to estimate.

ii. Medium Particles ($r \cong 100$ nm): As in the case for small particles, sufficient energy to vaporize is absorbed in 6 ns. Vapor will stream out to one mean free path in less than 1 ns; at this time the number density of carbon molecules will be much larger than the background gas density (specifically, about seventy times the background density if the average molecule contains three carbon atoms). Consequently we will assume that strong absorption continues until the vapor shell has time to expand to about ten mean free paths, say 20-50 ns. In this case, the carbon vapor may absorb several times as much energy as required to vaporize the original particle, raising the possibility that shock waves and ionization will be generated. Each of these processes can distribute thermal energy much faster than ordinary thermal diffusion.

iii. Large Particles ($r \cong 1000$ nm): The larger particles require much longer to vaporize, because the rate of energy absorption per carbon atom is lower, as indicated by Eqs. (1) and (5). This behavior can be interpreted as the result of shielding of the inner atoms; i.e., carbon particles with radii $>$ 100 nm are optically thick. Thus a 1000 nm radius particle will not vaporize over the duration of a typical CARS pulse (10 ns). However, the ratio of vaporization rate to surface area is of the same order as for a 100 nm particle; therefore, the very high density and initial rate of expansion found for a 100 nm particle is also encountered for larger particles. In fact, if the particle approaches complete vaporization the vapor shell must expand to approximately one hundred mean free paths before the carbon molecule density drops well below the average combustion gas density. Thus we estimate that absorption will continue for 100-200 ns (if the pulse lasts that long). The consequent high temperatures suggest a strong likelihood that shock waves and ionization will be generated.

H. Measurement Perturbations From Soot Absorption

Only about 10% of the soot vaporization energy is taken up as kinetic energy of vapor molecule translation, vibration and rotation. Recovery of the rest depends on the relative magnitudes of energy released in subsequent exothermic chemical reactions compared to the latent energy absorbed in vaporization. If these balance, and equilibrate over the measurement zone in a time short compared to the laser pulse, measurements of temperature will be perturbed by the relative amount

$$\frac{\Delta\theta}{\theta} = \frac{\phi \rho_c L}{\theta C \rho_g} \sim 1 \cdot 10^5 \, \phi \qquad (24)$$

for $L = 7 \cdot 10^4$ J/g. Here ϕ is the soot volume fraction. This rough estimate gives a fairly small perturbation for volume fractions of 10^{-9} to 10^{-6} typical, at least, of premixed flames[11].

Eckbreth[10] reasoned that even this perturbation could not be transmitted to a large fraction of the gas volume by ordinary heat conduction during a short laser pulse (~ 10 ns), except possibly in the case of a very large volume fraction and very small particles. In that case, the interparticle spacing is sufficiently small (~ 1 μm) to allow significant heat conduction in 10 ns.

However, we have noted the possibility that larger particles ($R \geq$ 100 nm) can absorb more than the energy necessary for vaporization, and consequently can generate shock waves and ionization. Each of these processes can transmit energy over distances of 10 micrometers or more in a few ns. Consequently, the possibility of measurement perturbation needs to be examined carefully in the case of large particles, even for the short pulses characteristic of CARS measurements. However, it is clear that CARS presents less chance of measurement perturbations; although the peak power densities encountered in typical CARS and single pulse Raman scattering measurements are about equal, the longer pulse required in typical Raman scattering measurements allows much more time for absorbed energy to affect measured quantities, while the greater energy requirements increase the potential magnitude of these effects.

I. Optical Background From Soot

The optical background created by ordinary thermal emission from soot, and the emission from laser-heated particles, can be calculated by using the absorption cross section to determine the optical absorption of the soot region over the path length z viewed by the Raman scattering receiving channels. This absorption is equal to the soot emissivity ε over the same path length. Thus

$$\varepsilon = 1 - \exp\left[- \frac{3z\beta\phi}{4r} \left(\frac{r}{\delta}\right) \right] \cong \frac{3z\beta\phi}{4r} \left(\frac{r}{\delta}\right) \qquad (25)$$

where the approximation is valid when the resulting emissivity is much less than one, and the factor in parentheses is omitted for large particles. (We assume for simplicity that the particles are all either "small" or "large".) For example, a 5 cm thick region with a small particle soot volume fraction of 10^{-7} will have emissivity

$$\varepsilon \cong 0.034$$

while if the particles are all large, say 1000 nm radius, the emissivity will be

$$\varepsilon \cong 0.0034$$

The spectral brightness of thermal emission from soot in this region in units of watts/(cm^2 nm sr) is

$$B_T = \varepsilon H_\lambda \tag{26}$$

where H_λ is the Planck function. Assuming a soot temperature of 1500K, we find that the thermal emission brightness at 550 nm is

$$B_T \text{ (550 nm, 1500°K)} = 2 \times 10^{-7} \text{ watts/(cm}^2 \text{ sr nm)}$$

for the small particle range assumed above. Notice that the brightness is a factor of ten smaller for the same volume fraction of large (r = 1000 nm) particles.

In comparison, the brightness B_R of the Raman scattering can be calculated by assuming (for simplicity) that the incident beam has a rectangular cross section of width W and depth D (in the direction of the collection optics). Then

$$B_R = \frac{PN_M\sigma_R}{W\Delta} \tag{27}$$

where P is the incident laser power, N_M is the molecule number density for the observed species and initial state, σ_R is the corresponding Raman scattering cross section and Δ is the Raman scattering line width. Using the representatives values P = 10^6 watts, W = $3 \cdot 10^{-2}$ cm, $N_M = 2 \times 10^{18}$ cm^3, Δ = 1 nm and $\sigma_R = 5 \times 10^{-31}$ cm^2/sr, we find

$$B_R = 3.3 \times 10^{-5} \text{ W/cm}^2 \text{ sr nm} \tag{28}$$

In this case the spectral brightness of the Raman scattering is about 150 times greater than the soot thermal emission. On the other hand, at a soot temperature of 2000K, the Raman scattering and soot emissions are about equally bright for a volume fraction of 10^{-7} and a viewed region of 5 cm thickness. Since the Raman scattering cannot be made much brighter without danger of laser breakdown of the gas, these estimates illustrate rough limits for Raman scattering visibility against intrinsic soot thermal emission as a function of soot size distribution, volume fraction, temperature and path length.

In many cases, a more stringent limit is set by the laser-induced soot heating. If the particles are heated to 5500K by the laser beam, the laser-induced brightness is given by

$$B_I = \varepsilon' H_\lambda (\Theta) f \tag{29}$$

Here ε' is the emission for the laser-heated region

$$\varepsilon' = \frac{3D\beta\phi}{4r}\left(\frac{r}{\delta}\right) \tag{30}$$

and f is the fraction of the pulse over which the laser-induced emission persists (ranging from ~1 % for small particles to > 10% for large ones for a one microsecond, 10^9 W/cm^2 pulse, according to our previous arguments concerning particle vaporization). Assuming $D = 3 \cdot 10^{-2}$ cm also, we find for $\phi = 10^{-7}$

$$\varepsilon' = 2 \times 10^{-4} \quad (\lesssim 100 \text{ nm})$$

$$\varepsilon' = 2 \times 10^{-5} \quad (1000 \text{ nm})$$

Then the laser-induced brightness is

$$B_I = 4 \times 10^{-6} \text{ W/cm}^2 \text{ sr nm} \quad (r = 5 \text{ nm}, f = 1\%, \theta = 5500^\circ\text{K})$$

$$B_I = 4 \times 10^{-5} \text{ W/cm}^2 \text{ sr nm} \quad (r = 100 \text{ nm}, f = 5\%, \theta = 6500^\circ\text{K})$$

$$B_I = 2 \times 10^{-5} \text{ W/cm}^2 \text{ sr nm} \quad (r = 1000 \text{ nm}, f = 20\%, \theta = 7000^\circ\text{K})$$

These results suggest that the laser-induced soot incandescence should not constitute a serious background for the smallest soot particles and will be comparable to the Raman scattering in the presence of larger particles. (Our calculations are somewhat more optimistic than those presented in Reference 10 because there appears to be an error overestimating the radiation from particles by a factor of ten in those references, and because we have taken into account particle vaporization.) However, the simplicity of the approximations used to draw these conclusions makes them uncertain. In particular, uniform light intensity in time and space has been assumed. In practice, the beam is weaker early in the pulse and along its boundaries. Since the particle temperature and thermal emission are weak functions of beam intensity, the thermal emission will be fairly uniform across the beam. However, the particles will vaporize much more slowly in the weaker flux times and regions. This behavior will increase the factor f and intensify the laser-induced background problem.

In practice, a sharp drop in laser-induced emission has been seen by Eckbreth[10] during a several microsecond pulse at incident intensities greater than 10^7 W/cm^2. The peak durations are consistent with size distribution measurements which indicated a preponderance of larger particles. The persistent luminescence could be due to slow vaporization of larger particles, or particles on the edge of the laser beam. Alternately, it could be fluorescence from reaction products of the vaporized carbon with surrounding molecules, or, as Eckbreth suggests, it could arise from an observed thermal defocusing of the beam within the dye laser used for his experiments. The latter process would expose new soot particles during the latter stages of the pulse.

Our experiments indicate laser-induced luminescence levels approximately ten times the Raman scattering signal in incipient sooting regions of the rich premixed propane air flame. Volume fractions and particle sizes in this region have not been determined yet, nor has the time dependence of the laser-induced radiation been measured. However, the soot volume fraction should be lower than 10^{-7} in this region because the orange glow characteristic of soot emission was just becoming visible. It is possible that the predominant background emission here is fluorescence from soot precursors. We cannot draw reliable conclusions about the source of observed background in our experiments until the time and spectral dependence of this radiation is studied as a function of laser power. The fluorescence intensity is expected to follow the laser pulse fairly closely, while the emission from small soot particles should drop off sharply as the soot vaporizes. Because the anti-Stokes fluorescence at large shifts should arise mostly from multiple photon events, it should vary more rapidly with laser power than induced thermal emission.

J. Methods of Minimizing Laser-Induced Soot Incandescence Backgrounds

Whether or not our observations were of soot emission, analysis of the laser-induced soot luminescence indicates that Raman scattering will face comparable to stronger background in the more dense soot regions. There are several ways which have been suggested to relax this limitation. Eckbreth[10] has tried rapid alternation of the laser beam polarization during the pulse using a Pockels cell driven by a sine wave. The soot emission should not be changed by this oscillation, but the Raman scattering should follow the oscillation because of its strong polarization dependence. A filter passing only the polarization modulation frequency should then separate the Raman signal from the unmodulated background due to soot luminescence (or quenched fluorescence). To our knowledge, this approach has been demonstrated but not tried extensively, probably because it reduces the effective laser energy by a factor of at least two, and does not provide sufficient discrimination in practical implementation.

We have attempted to use conditioned sampling approaches to circumvent this laser-induced background problem in turbulent diffusion flames. One approach involved setting the detection electronics (or

computed analysis program) to omit all signals larger than a threshold value set larger than any possible Raman signal. This permitted good Raman data to be collected from clean flame zones under conditions where sooty regions were oscillating in and out of the optical detection zone. This form of conditioned sampling can provide valid temperatures and major species concentration data in unsooty flame pockets and a measure of the relative number of soot versus nonsoot containing pockets at that flame location.

In a second conditioned sampling approach, the pulsed Raman laser was triggered only when scattering from a probe cw laser indicated the absence of large soot particles in the sample zone. This technique was not successful because no strong particle scattering from a 4 watt cw laser could be detected in sooty flame zones, even though the sensitivity of the channel was sufficient to see 10^6 detected photons/sec from Raleigh scattering. The lack of Mie scattering pulses indicated that only soot particles smaller than 0.1 μm were present. This form of conditioned sampling does not appear to be a promising general approach for these sooting flame regions because the distribution of background producing constituents appears to be homogeneous. However, in sections of the flame further downstream or in other flames where a few large soot particles may be present, this technique may be useful.

Alternately in approaches that we have not tried experimentally, the effective soot emission might be reduced in regions of smaller particles by gating the detection system to look only at the latter part of the pulse, after the particles are vaporized. Finally, an approach which seems the most widely applicable is to vaporize the soot particles by a laser prepulse. From Eq. (13) only 7 J/cm^2 (or 70 mJ in a 1 mm^2 cross section beam) is required to reduce the volume fraction of smaller soot particles to 5% of its original value. In this case, a larger laser pulse following several microseconds later will probe a region which is relatively particle-free. The success of this approach requires weak fluorescence from molecules formed by the excess carbon and insignificant perturbation of the measured quantities by particle vaporization. A more detailed analysis and experiments in this area are clearly worthwhile.

K. Measurement Perturbation and Background From Molecular Absorption and Fluorescence

In addition to soot precursors, a number of other molecules found in combustion gases have significant absorption cross sections in visible light bands. Among these are C_2, C_3, CH, CN, NO_2 and OH. Although these are nearly always minor constituents, only a small amount of absorption is necessary to perturb the gas temperature significantly. The equilibrium temperature rise is given by

$$\Delta\theta = \frac{Q_o k}{C\rho_g} \tag{31}$$

where Q_o is the integral of the power density over the duration of the laser pulse. The molecular absorption coefficient is given by

$$k = N_M \sigma_{ABS}$$

where N_M is the number density of absorbing molecules, and σ_{ABS} is the corresponding absorption cross section per molecule at the laser wavelength. For our single pulse Raman measurements, $Q_o \sim 10^3$ J/cm^2. Substituting values of C and ρ_g for high temperature nitrogen:

$$C = 1.3 \text{ J/g}^\circ\text{K},$$

$$\rho_g = 2.4 \times 10^{-4} \text{ g/cm}^3,$$

we find

$$\Delta\theta = 3.3 \times 10^6 \text{ (cm}^\circ\text{K)}k.$$

Thus, even absorption corresponding to an optical mean free path (63% absorption) of 100 m can produce a 330K temperature rise in flame gases. This level of absorption would be created by molecules having an absorption cross section of 10^{-18} cm^2 at concentrations of about 20 ppm. If the absorbed energy is communicated to measured quantities, such as the vibrational excitation of N_2 during the laser pulse, significant measurement perturbation will result. However, this effect could be mitigated by the bleaching tendency of the intense laser beam to saturate the absorbing species and to excite or dissociate the absorbing molecules into nonabsorbing species.

In addition to causing possible measurement perturbation, some of the light absorbed by molecules is reradiated in the form of fluorescence. Typically, the re-emitted fraction is very small, on the order of 10^{-4} or less, because most of the energy is degraded by collisions before emission can occur. Nevertheless, the re-emitted fraction can provide a significant background to Raman scattering. For example, if the mole fraction, X_A, of the absorbing species in molecular states leading to absorption of the laser radiation is 10^{-6}, the mole fraction, X_R, of the observed Raman species is 0.1, the absorption cross section is 10^{-18} cm^2, and the re-emitted fraction, F, in the Raman bandwidth is 10^{-6}, then the ratio of Raman scattering to the fluorescence background is

$$R = \frac{4\pi X_R \sigma_R}{X_A \sigma_{ABS} F} \approx 1.3 \times 10^{e0} \text{ (cm}^2 \text{ sr)} \ \sigma_R \qquad (32)$$

Since typical Raman scattering cross sections of importance here are on the order of 10^{-30} cm^2/sr, this estimate indicates the possibility of strong interference from a relatively minor species. However, the prediction can be pessimistic for several reasons. First, the absorption cross sections for small molecular species reach 10^{-18} cm^2 only in confined bands, which often can be avoided using a tuned laser source. Second, the bleaching effects of high intensity laser beams mentioned previously can reduce fluorescence commensurate with absorption. Third, methods distinguishing against fluorescence are available, including Raman scattering measurements confined to the anti-Stokes side, and the polarization modulation described previously.

In practice, Leonard[13] and Yaney[14] have identified fluorescence background using UV excitation (337 nm) in jet turbine exhaust gas. Fluorescence excited by cw 488 nm radiation, apparently originating from pyrolyzed fuel (soot precursors) was observed by Haynes[11], and Eckbreth[10] inferred the presence of C_2 fluorescence associated with soot vaporization. On the other hand, we have not observed significant fluorescence background in our Raman scattering measurements on hydrogen-air flames and light hydrocarbon premixed flames (methane, propane), except possibly in incipient sooting regions of the rich propane flame.

V. COMPARISON OF RAMAN SCATTERING AND CARS FOR TURBULENT COMBUSTION MEASUREMENTS

A. Characteristics of CARS

CARS is the most developed of several nonlinear optical processes[15-17] that have received considerable attention for combustion analysis since its initial application to flames eight years ago[18]. Compared to spontaneous Raman scattering, CARS has two major advantages — increased signal intensities and a collimated output.

To discuss the signal levels attainable in an idealized case, we assume collinear monochromatic pump and Stokes beams overlapping in a diffraction-limited focus. For this case, the anti-Stokes signal power is given by

$$P_{AS} = \left(\frac{2}{\lambda_p}\right)^2 \left(\frac{8\pi^3}{c\lambda_{AS}}\right) P_P^2 P_S |x|^2 \tag{33}$$

where λ is the light wavelength, P is the power of each indicated beam, and x is the third order nonlinear susceptibility. When λ_S is tuned to equal the wavelength of an isolated, homogeneously broadened Raman line,

$$x = \frac{i\lambda_S^6}{16\pi^5 hc} \frac{N_j \sigma_j}{\gamma_j} \tag{34}$$

Here N_j is the concentration difference between the upper and lower molecular states involved in the transition, σ_j is the Raman scattering cross section, and γ_j is the Raman linewidth in wavelength units. Typical values found in combustion measurements are:

λ_P = 500 nm
λ_S = 566 nm (N_2 vibrational Q-branch)
λ_{AS} = 448 nm
N_j = 10^{17} cm^{-3} (for a particular rotational contribution to the vibrational Q-branch)
σ_j = 5×10^{-31} cm^2/sr
γ_j = 5×10^{-3} nm
P_P = 1 MW
P_S = 0.1 MW

For these values, $P_{AS} \cong 30W$. In comparison, the overall Stokes Q-branch ordinary Raman scattering from 1 mm pathlength and comparable incident beam power will be about 10^{-6}W. For a fair comparison, we should include the contribution to the CARS signal from the other rotational components of the Q-branch (increasing the CARS power by a factor ~ 10), take into account that beams used in pulsed CARS measurements are rarely diffraction-limited (decreasing the CARS signal by several orders of magnitude), and note that typical Raman scattering pulses will persist for about one hundred times longer than the pulse used for CARS (increasing the total energy in the Raman scattering signal). Nevertheless, even with the lower signal strength inherent in the CARS configuration most used in single-pulse combustion measurements (BOXCARS[19] with at least one broadband laser), CARS offers approximately 10^3 total signal advantage over Raman measurements for major species.

Secondly, the CARS signal is collimated in a beam with a divergence similar to that of the incident laser beams. This permits nearly all of the CARS signal to be collected, versus only about 1% for the nearly isotropically scattered spontaneous Raman signals. This is particularly important in probing complicated combustors whose design can permit double ended optical access required for CARS, but which often do not tolerate the large apertures or windows necessary for efficient Raman collection. The collimated CARS output also greatly enhances (typically by four to six orders of magnitude) background rejection of blackbody radiation from combustor walls, soot incandescence, or laser-induced fluorescence.

However, CARS does have significant disadvantages compared to Raman scattering, discussed in the following paragraphs. These include:

1. More costly and complex experimental configuration;
2. Much more sophisticated data analysis;
3. Sensitivity to laser power and beam quality fluctuations, turbulence effects, and background gas compositions; and
4. Difficulty in simultaneously measuring several molecular species.

CARS requires the interaction of two laser beams. In combustion measurements, the pump beam is often split and crossed (BOXCARS) to increase spatial resolution[20]. For time-averaged measurements, both lasers can have narrow frequency outputs, and the CARS spectrum is generated by sweeping the frequency of one of the lasers. For single-pulse measurements, an alternative approach is required using a multichannel detector and one broadband laser which spans a wavelength range broader than the Raman band of interest. Both the BOXCARS and broadband configurations decrease the generated signal intensity and increase experimental complexity.

Analysis of CARS data to determine temperature or species concentration requires a considerable amount of calculation. Unlike spontaneous Raman processes where the intensities of many closely spaced lines (i.e., rotational lines in a vibrational Q-branch) can be summed to calculate the total intensity, individual CARS resonances interfere with each other and with background gas nonresonant contributions. The effect of these interferences depends on the Raman linewidth, which in turn is a function of background gas composition, pressure and temperature. Thus the CARS spectrum is a complicated function of molecular energy levels, temperature, pressure and Raman line widths. It has been found necessary to have an accurate prediction of the spectrum under various conditions in order to determine temperature or molecular species concentration. Fortunately, theoretical CARS spectral calculations in agreement with experimental measured spectra have been made for many diatomic molecules as well as for H_2O[21-23].

CARS temperature measurements are obtained from the ratio of signal intensities in two or more spectral bands. Since band ratios are less sensitive to the effects discussed above than individual band intensities, accurate CARS temperature measurements appear to be obtainable under many conditions encountered in practical combustors and in fact, several examples of such measurements have been reported.

On the other hand, the most direct way to measure major species concentrations is in terms of their absolute band intensities (or intensities relative to a standard). Eq. (33) indicates that the integrated CARS signal depends roughly on the cube of the overall laser pulse energy (assuming P_S proportional to P_P and constant pulse shapes). Thus, modest laser pulse energy fluctuations can cause large pulse-to-pulse CARS signal fluctuations.

In addition, CARS absolute signal intensities depend strongly upon the spatial, spectral and detailed temporal dependence of the incident laser beams. In standard CARS combustion measurement configurations, the pump and Stokes beams are generated by two separate lasers. Although the Stokes laser is usually pumped by a fraction of the pump laser beam, each laser displays partially uncorrelated spatial and temporal structure. Analysis of the time dependence of the input laser beams and CARS output signal using a very fast photodiode has demonstrated that large variations in the shape of the Nd:Yag pump laser pulse occur due to longitudinal mode beating. The interaction between the mode beating of the Nd:Yag pump and the Stokes dye laser accounts for much of the temporal modulation of the CARS intensity.

The combination of these effects in CARS signal production has been described successfully in theoretical studies only with simplified models of the laser emission[24, 25]. However, experiments have demonstrated the significance of these effects. In room temperature studies of still laboratory air, 50%-70% shot-to-shot fluctuations in CARS signal intensities have been observed[26] even after correction for overall pulse energy fluctuations. These fluctuations can be reduced by

directing part of the incident laser beams through a reference cell containing the gas at known pressure and temperature and normalizing the observed CARS intensity in the sample by that simultaneously measured from the reference cell. Goss and Switzer[27] have reported reduction to 10%-20% in still air by careful balancing of the optical elements and pathlengths in the reference and signal legs.

Since, in many cases, signals arising from major species will be proportional to the square of the species concentration, this fluctuation corresponds to ca 5%-10% uncertainty in the concentration of those species. Some additional improvements have been obtained by use of a single longitudinal mode Nd:Yag laser[27], and further refinements of reference cell balancing. Thus, using these techniques, CARS has been shown to provide excellent concentration measurements in still (or nonturbulent) gases. However, many applications require that the measurement zone be viewed through a turbulent flow.

In a turbulent gas, local variations in refractive index (which can arise from fluctuations in concentration and temperature) alter the focal spot sizes, shapes and positions of the pump and Stokes beam. Goss and Switzer[26] have investigated the influence of these effects by introducing a turbulent helium flow in front of a still air measurement region. In one typical case, they found that the very strong turbulence introduced by this configuration reduced a collinear CARS signal by a factor of eleven. Calculations based upon an approximate turbulence model for a flame indicated that appreciable collinear CARS signals fluctuations should be expected when the beams must traverse several tens of centimeters or more of turbulence to the measurement zone. For BOXCARS, the sensitivity to turbulence is greater because the beams traverse significantly different paths to the measurement zone.

Several schemes to remove turbulence effects in concentration measurements have been investigated. Goss measured the nonresonance CARS signal separately, and used this in-situ reference to correct for beam defocusing. Shirley et al[28] found that interference between the resonance and nonresonance CARS signals can be used to determine concentration from band shape rather than band intensity, converting the concentration determination from an absolute intensity to a relative intensity measurement. This interference occurs naturally for intermediate species, and can be induced for major species by polarization techniques. Both approaches appear to provide strong correction of turbulent CARS fluctuations in favorable cases (strong nonresonance signal) but suffer from weak signal effects under many combustion conditions, making single pulse measurements difficult. Furthermore, both methods require at least approximate knowledge of the in-situ nonresonance cross section. Although this cross section is approximately constant in combustion products of varying composition, it can vary strongly in fuel-rich regions.

Thus the present evidence suggests that reliable single pulse major species turbulent concentration measurements can be obtained over short

distance, up to perhaps 10-30 centimeters for collinear CARS, without turbulence compensation. In other turbulent configurations, in-situ references or line shape analysis, both using nonresonance CARS contributions, appear to provide useful compensation for turbulence effects under favorable conditions but are not yet generally applicable for single pulse combustion measurements.

One of the advantages of Raman scattering not shared by CARS is the ability to measure temperature and a number of molecular species concentrations simultaneously using only one laser in a straightforward fashion. Straightforward application of CARS for multiple species measurements presently would require an additional laser beam and detector for each additional molecular species. However, recently reported observations of rotational CARS may point the way toward relaxed laser requirements for multiple species measurement, since in rotational CARS transitions from many molecular species occur in a relatively narrow wavelength range which can be covered by one broadband Stokes laser. Until recently, the problem with this approach has been separating the rotational anti-Stokes lines from the pump beam, since they lie relatively close to it spectrally and sufficiently strong spectral discrimination is difficult to achieve over a small wavelength span[29, 30]. This problem has been relaxed by the demonstration of a folded BOXCARS configuration[28] in which the Stokes beam is placed in a plane perpendicular to that defined by the two pump beams. In this case, it can be shown that the CARS beam is well separated in direction from the pump and Stokes beam. Thus one can obtain strong spatial discrimination against those beams, relaxing the need for strong spectral discrimination.

B. Nonsooting Laboratory Flames

Table 5 compares the capabilities of pulsed Raman scattering and CARS for diagnostic measurements in clean, laboratory-scale turbulent flames. The Raman characteristics have been experimentally measured in our laboratory using pulsed Raman measurements on premixed, laminar and nonpremixed turbulent H_2-air and propane/H_2-air flames. Characteristics of CARS are "best values" obtained from the literature and represents work done by a variety of researchers.

The spatial resolution is essentially identical (a cylinder ~ 0.6 mm long and 0.1 mm in diameter) for Raman and for BOXCARS[31]. The differences in temporal resolution and repetition rate listed in Table 5 are not inherent characteristics, but reflect the type of lasers commonly used for each technique. For pulsed Raman scattering where pulse energy is the most important factor, flash lamp pumped dye lasers are often employed. The 2 μs and 1 pps values in Table 5 correspond to our current laser facility which has an output power of ~ 1 J/pulse. Sandia National Laboratories (Livermore) Combustion Research Facility has a larger flash-lamp-pumped dye laser which not only has increased power (5 J/pulse) but a higher repetition rate as well (10 pps). In CARS , where peak pulse power is the critical parameter, Nd:Yag lasers with pulse

widths of 10 ns and repetition rates of 10 pps are the most commonly utilized.

i. Temperature Measurements. Pulsed Raman measurements of laminar, premixed H_2-air flames discussed in Section II have demonstrated an experimental average value accuracy of 50K with a single pulse measurement standard deviation of 4%. Accuracies are limited by system calibration and background subtraction errors while precisions are photon-noise limited.

Temperature can be determined from CARS intensity ratios from two vibrational bands of N_2 or from comparison of N_2 vibrational CARS band shapes with computer calculated spectra as a function of temperature. Since these procedures require only relative CARS intensity measurements and the entire N_2 vibrational spectrum can be obtained for each laser shot using a broadband Stokes laser and a multichannel detector, they are relatively insensitive to laser beam fluctuations, turbulence effects and local molecular environments. Temperatures determined from band analysis of CARS N_2 spectra agreed within 50K with temperature measured by NaD line reversal and radiation corrected thermocouples in laminar premixed flames[32]. A BOXCARS optical configuration was used to insure a small sample volume. However, the CARS spectra were generated by slow spectrometer scans requiring many laser pulses.

CARS spectra can be obtained with both high temporal (single laser pulse) and high spatial (BOXCARS) resolution, as has been demonstrated by Eckbreth for laminar premixed[32] and laminar diffusion flames[31]. However, no values of precision for these single shot data were stated. Goss et al[26] have used a collinear CARS configuration (large sampling volume) to obtain temperatures from single laser shots in a premixed propane/air burner. The results of eighteen independent measurements were 2144 ± 140K. The average temperature obtained was 100K higher than the average temperature determined by sodium D line reversal. The precision (± 140K) indicates a 7% standard deviation, which may be further degraded when going to a BOXCARS configuration since BOXCARS intensities are typically lower than collinear CARS by one or two orders of magnitude[20,27]. The precision of a set of temperatures from temporally and spatially resolved CARS data from a laminar flame remains to be verified experimentally, as well as the effect of refractive index changes in turbulent flame environments.

ii. Concentration Measurements. Concentration measurements of major flame species can be measured in a single laser shot with Raman scattering, as this study has demonstrated (see Sections II and III). All major flame species (i.e., H_2, N_2, O_2 and H_2O) were measured simultaneously with standard deviation in the most favorable cases of ± 4%. As in Raman temperature measurements, the accuracy of concentration values are limited by calibration and background subtraction errors while the precision is photon-noise limited. The lower limit of concentration

that can be reliably determined with a single laser pulse is ~ 0.01 mole fraction, limited by background subtraction uncertainties. This concentration limit can be lowered (to ~ 100 ppm) for time averaged measurements if detailed spectral scans using a multichannel detector or multiple laser shots are taken to measure the background more accurately and if multiple laser shots are averaged to decrease the photon noise.

Concentration measurements for CARS intensities are more difficult to obtain quantitatively and are the subject of much current research. In early work using reference cells, CARS was used to measure H_2 concentration profiles in a premixed natural gas/air flame[18]. However, this work is only qualitative in that no temperature dependent corrections were made for line width or population distribution changes[15]. Single mode laser and reference cells were used to measure nitrogen and oxygen concentration (with background cancellation using polarization techniques) concentration in a premixed propane/air flame[26]. After temperatures were determined, concentrations were measured by integrating the entire Q-branch, a procedure which neglects the dependence of Raman cross section and line width on the rotational quantum number J as well as the affects of any nonresonant backgrounds. Although no quantitative analysis has established the errors inherent in this method, an average concentration measurement accuracy of better than 5% (or 0.03 mole fraction) was quoted for N_2.

The shape of the CARS profile has been used to follow CO[17, 33] and O_2[33] concentrations in flames. Good agreement between measured CO determined by CARS and by probe sampling was obtained at the $X(CO_2) = 0.04$ level[33].

The capability of single pulsed CARS measurements of N_2 concentration and of simultaneous temperature and N_2 concentrations have been reported[26] from a premixed propane/air flame although the results were not analyzed. Eckbreth[15] has estimated that using in-situ nonresonant background[34] or band shape analysis[33] that single pulse concentration measurements with a precision of ± 10% are possible. This is an area of active research interest[26, 28, 34] and the capabilities and limitations of concentrations measured by time- and space-resolved CARS techniques may soon be more fully known.

Because of the much larger signal intensities for CARS compared to Raman scattering from major flame species, one might expect that CARS would be capable of measuring minor flame species. However, this is not true because CARS intensities depend on the square of the concentration of the observed species (Eqs. 33 and 34) and its signal diminishes rapidly into the nonresonant background with decreasing concentration.

Experimentally, both background subtraction techniques and band shape analysis techniques appear to be approximately comparable in sensitivity[28] with a minimum CO detectability of ~ 0.01 mole fraction in high temperature flame zones and 0.001 in lower temperature regions. A theoretical comparison of detectability[35] limits for background subtraction CARS and Raman scattering concluded that Raman scattering was more sensitive in clean flames but that this superiority was rapidly degraded in luminous flame environments.

Our conclusion is that pulsed Raman scattering is preferable to CARS in clean laboratory scale turbulent flame studies primarily because single pulse concentration measurements from Raman scattering are more accurate, more precise, and can easily yield simultaneous multispecies information. However, CARS is an extremely useful technique for studying laboratory systems which are not amenable to Raman scattering.

C. Sooty Flames and Practical Combustors

The range of applicability in turbulent combustion for Raman scattering and CARS is summarized in Table 6. As demonstrated in this study, pulsed Raman scattering is well-suited to laboratory scale H_2 and hydrocarbon flames. However, in the presence of soot, large laser-induced backgrounds can make this technique unsuitable, although application of Raman scattering to larger scale (more practical) combustors have been successful to a limited extent. Examples include jet engine exhaust[36, 37], stratified charge engines[38], internal combustion engines prior to ignition[39, 40] and combustion tunnels[14, 41]. However, these applications often would be limited to certain fuels, fuel-to-air ratios, combustor zones or times in the combustion cycle when Raman measurements were possible.

CARS, because of its much stronger inherent signal intensity and collimated output, is much more immune to the background interferences (i.e., luminescence, soot incandescence, fluorescence) which can make Raman measurements impossible. Lower laser energies are required for CARS, minimizing sample perturbations arising from particle or molecular absorption. In addition, although the optical access necessary for CARS is double-ended, only narrow aperture windows are required, which are often more compatible with practical combustor designs than a larger aperture window necessary for efficient collection of Raman scattering. These capabilities of CARS are demonstrated by its recent application to temperature measurements in sooting propane diffusion flames[31], the exit plane of a kerosene burner[42], a bluff body stabilized propane diffusion flame combustor[43], an engine cylinder[44], and in the primary use of a swirled, coannular burner with Jet A liquid fuel and the exhaust of a JT-12 combustor can[45].

VI. SUMMARY

Vibrational Raman scattering has been shown to be a reliable, quantitative method for instantaneous, simultaneous measurement of temperatures and molecular species concentrations in a variety of laboratory scale flames. Results with a 1J/pulse laser on laminar, premixed H_2-air flames demonstrate a low measurement uncertainty for temperature (4% standard deviation) and major species concentration due almost entirely to theoretically predicted photon statistical fluctuations. All major flame species (H_2, O_2, N_2, H_2O) are measured simultaneously and other molecular species can be added with minor experimental changes. The excellent agreement with theory for concentration and with thermocouple results for temperature demonstrate that systematic Raman measurement errors are acceptably low (1 mole fraction percent and 40K) with current calibration techniques.

Results of pulsed Raman studies of turbulent flames indicate no added difficulties. Valid measurements with a temporal resolution of 2μs and a spatial resolution of $\sim$0.1 mm^3 are obtained in all parts of the flame including mixing layers of H_2-air turbulent jet diffusion flames where large fluctuations exist (i.e., temperatures ranging from 300-2400K at a given flame location). Comparisons with adiabatic flame calculations demonstrate the importance of differential diffusion in mildly turbulent H_2-air flames, and the Raman data was subsequently used to validate advanced models which include differential diffusion effects. [9]

The major limitations of pulsed Raman scattering are high laser-induced optical background signals which were observed in sooty, hydrocarbon flame regions and which precluded meaningful Raman measurements. Measurements in nonsooting propane-air flames demonstrate that flame luminosity is not a problem because the gated electronics automatically subtract this background. However, in sooty regions of premixed laminar or non-premixed turbulent propane-air flames, background signals caused by laser-induced particle incandescence or molecular fluorescence are dominant.

An analytical study of these processes suggests that soot, in the presence of the high flux laser pulses ($\sim 10^9$ watts/cm^2) necessary for Raman or CARS, rapidly reaches vaporization temperatures of about 4000K, radiating thermally at this elevated temperature until it disappears by vaporization. Calculations of intensity of this laser-induced soot incandescence suggest that it will not be a serious background for small (r=5nm) soot particles and will be comparable to Raman scattering intensities in the presence of larger ($r \sim 1000$nm) particles. This calculation is somewhat more optimistic than the analysis in Ref. (Eckbreth) because there appears to be an error overestimating radiation from particles by an order of magnitude in that reference and because we have taken into account particle vaporization.

In addition to high optical backgrounds, this laser-induced soot incandescence and vaporization process can cause serious sample perturbations. The vaporizing particle produces a plume of predominantly carbon vapor which can by collisions transfer energy to N_2 and other gas molecules (perturbing temperatures based upon N_2

vibrational populations) or react with the surrounding gas, further changing its composition and temperature. The rates of energy transfer and chemical reaction may be slow enough to cause limited effects for CARS measurements made on a 10ns timescale, but may not be insignificant for pulsed Raman measurements with a microsecond temporal resolution.

Several methods of circumventing soot incandescence (permitting the possible application of pulsed Raman scattering to some sooty flame environments) are suggested based upon conditioned sampling data collection (and/or analysis) or double pulse laser techniques.

In general, however, coherent anti-Stokes Raman scattering (CARS) appears to be a better choice for sooting flames because the shorter laser pulses and somewhat lower laser energy requirements minimize soot incandescence and potential sample perturbation effects and because its collimated signal output permits excellent rejection of the laser-induced background. The collimated output and larger signal intensities inherent in CARS give it significant additional advantages over Raman scattering for temperature measurements in large scale combustors since large optical access is not required for efficient signal collection (small aperature double-ended optical access is still required however) and thermal radiation from combustor walls is more easily rejected.

However, for studies of nonsooting laboratory flames, Raman scattering is generally preferable to CARS. Both concentration and measurements determined from Raman measurements are essentially photon noise limited. Concentration measurements based upon CARS data are much more dificult to quantify. Methods for improving precision in concentration measurements are under active investigation and include single mode lasers and reference cells, ratioing CARS intensities to simultaneously measured non-resonant CARS emission intensities, and bandshape analyses of the interferences of the resonant and non-resonant susceptibilities. Precisions for single pulse concentration values measured by these advanced CARS techniques have not been firmly established but are estimated to be higher (i.e., less precise) than those attainable by RS. For temperature measurements the accuracy of RS and CARS are essentially equal ($\sim$50K error), but the precision of single-laser-pulse temperature measurements are more firmly established for RS ($\pm$ 4% relative standard deviation) than for CARS.

Additionally, Raman scattering has the capability of measuring many different molecular species concentrations simultaneously using relatively simple equipment. Only a single laser is required an multiple species capability is obtained by adding a detector channel for each additional species. For example, in this study on H_2-air premixed and turbulent, nonpremixed flames temperature and concentrations of all major flame species (H_2, N_2, O_2, H_2O) were measured simultaneously for each laser shot. This information providing correlations and joint probability density functions, is extremely valuable as demonstrated in our analysis for differential diffusion effects.

For CARS, multiple species capabilities would generally require the use of several Stokes laser beams to span the spectral range for widely separated vibrational Raman lines and a number of detector channels

would be necessary for each species (or group of spectrally-close species neighbors) to properly correct for temperature and non-resonant background effects. (A possible new direction being considered for such multicomponent measurement capability is pure rotational CARS, which is in the early stages of study.)

Thus Raman scattering is preferable to CARS for measurements in clean, laboratory-scale flames. Indeed, if Raman scattering were several orders of magnitude more intense than it is, it would be the method of choice over CARS for nearly all combustion measurements. As it is, CARS provides the best choice in many combustion environments for which dominant problems exist concerning discrimination against intrinsic or laser-induced background, reduction of measurement perturbations, or application to combustors where optical access is limited to very small apertures. For these advantages, one must pay the price of some combination of additional overall experimental complexity, poorer accuracy and/or less simultaneous species concentration information (limiting for flame modeling efforts).

REFERENCES

1. M.C. Drake, M. Lapp, C.M. Penney, S. Warshaw, and B.W. Gerhold, AIAA Paper No. 81-0103 (1981).

2. J.H. Kent and R.W. Bilger, Fourteenth Symp. (Int.) on Combustion, The Combustion Institute, 1973, p. 615; R.W. Bilger, Combustion Sci. Tech. 13, 155 (1976).

3. M. Lapp, in Laser Raman Gas Diagnostics, M. Lapp and C.M. Penney, Eds., Plenum Press, New York, 1974, p. 107.

4. M.C. Drake, M. Lapp, C.M. Penney, S. Warshaw, and B.W. Gerhold, Eighteenth Symp. (Int.) on Combustion, The Combustion Institute, 1981, p. 1521.

5. M. Lapp and R.M.C. So, in AGARD Conference Proceedings No. 281 on Testing and Measurement Techniques in Heat Transfer and Combustion, 1980, Chapt. 19.

6. A.S. Gordon and B. McBride, "Computer Program for Calculation of Complex Chemical Equilibrium Compositions, Rocket Performance, Incident and Reflected Shocks and Chapman-Jouget Detonations," NASA SP-273, 1971.

7. R. Bilger, personal communication.

8. J.A. Miller and R.J. Kee, J. Phys. Chem., 81, 2534 (1977).

9. R.W. Bilger, AIAA Paper 81-0104 (1981).

10. A.C. Eckbreth, AIAA Paper No. 76-27 (1976); J. Appl. Physics 48, 4473 (1977).

11. B.S. Haynes, H. Jander and H. Wagner, Ber. Bunsenges Phys. Chem. 84, 585 (1980).

12. H.A. Jones, I. Langmuir, and G.M.J. Mackay, Phys. Rev. 30, 201 (1927).

13. D.A. Leonard, AFAPL-TR-74-100 (1974).

14. P.P. Yaney, "Combustion Diagnostics Using Laser Spontaneous-Raman Scattering," AFAPL-TR-79-2035 (1979).

15. A.E. Eckbreth, Eighteenth Symp. (Int.) on Combustion, The Combustion Institute, 1981, p. 1471.

16. J.W. Nibler and G.V. Knighten, in Raman Spectroscopy of Gases and Liquids, A. Weber, Ed., Springer-Verlag, 1979, Chapt. 7.

17. S. Druet and J.P. Taran in Chemical and Biological Applications of Lasers, C.B. Moore, Ed., Academic Press, 1980, p. 187.

18. P.R. Regnier and J.P.E. Taran, Appl. Phys. Lett 23, 240 (1973).

19. W.B. Roh, P.W. Schreiber, and J.P.E. Taran, Appl. Phys. Lett. 29, 174 (1976).

20. A.C. Eckbreth, Appl. Phys. Lett. 32, 421 (1978).

21. R.J. Hall, Comb. Flame, 35, 47 (1979).

22. W.M. Shaub, S. Lemont and A.B. Harvey, Appl. Spect. 33, 268 (1979).

23. R.L. St. Peters, AFWAL-TR-80-2062 (1980).

24. R.L. St. Peters, Opt. Lett. 4, 401 (1979).

25. M.A. Yuratich, Mol. Phys., 38, 625 (1979).

26. L.P. Goss, G.L. Switzer, and P.W. Schreiber, AIAA 80-1543 (1980).

27. M. Pealat, B. Attal, S. Druet, and J.P.E. Taran, in Laser Probes for Combustion Chemistry, D.R. Crosley, Ed., American Chemical Society, 1980, p. 25.

28. J.A. Shirley, R.J. Hall, J.F. Verdieck, and A.C. Eckbreth, AIAA 80-1542 (1980).

29. I.R. Beattie, T.R. Gilson, and D.A. Greenhalgh, Nature, 275, 378 (1978).

30. L.P. Goss, J.W. Fleming, and A.B. Harvey, Opt. Lett., 5, 345 (1980).

31. A.C. Eckbreth and R.J. Hall, Comb. Flame, 36, 87 (1979).

32. A.C. Eckbreth in Characterization of High Temperature Vapors and Gases, J.W. Hastie, Ed., National Bureau of Standards, 1979, p. 943.

33. J.A. Shirley, A.C. Eckbreth and R.J. Hall, in Proceedings of the 16th JANNAF Combustion Meeting, Monterey, CA., 1979; A.C. Eckbreth, Seventeenth Symp. (Int.) on Combustion, The Combustion Institute, 1979, p. 975.

34. R.L. Farrow, R.E. Mitchell, L.A. Rahn and P.L. Mattern, AIAA 81-0182 (1981); L.A. Rahn, L.J. Zych, and P.L. Mattern, Opt. Comm. 30, 249 (1979).

35. L.A. Rahn, P.L. Mattern, and R.L. Farrow, Eighteenth Symp. (Int.) on Combustion, The Combustion Institute, 1981, p. 1533.

36. D.A. Leonard, AVCO Everett Res. Lab, Research Note 914 (1972).

37. W.M. Rocquemore and P.P. Yaney, in Characterization of High Temperature Vapors and Gases, J.W. Hastie, Ed., National Bureau of Standards, 1979, p. 973.

38. J.R. Smith, in Laser Probes for Combustion Chemistry, American Chemical Society Symposium Series, Vol. 134, D.R. Crosley, Ed., American

Chemical Soc., Washington. D.C., 1980, p. 259.

39. R.E. Setchell, "Initial Measurements Within an Internal Combustion Engine Using Raman Spectroscopy," Sandia National Labs Report, SAND 78-1220, 1978.

40. S.C. Johnston, "Precombustion Fuel/Air Distribution in a Stratified Charge Engine Using Laser Raman Spectroscopy," Sandia National Labs Report, SAND 78-8707, 1979.

41. W.D. Williams, H.M. Powell, R.L. McGuire, L.L. Price, J.H. Jones, D.P. Weaver and J.W.L. Lewis in Turbulent Combustion, L.A. Kennedy, Ed., American Institute of Aeronautics and Astronautics, 1978, p. 273.

42. M. Pealat, J.P.E. Taran, and F. Moya, Opt. and Laser Tech., 12, 21 (1980).

43. G.L. Switzer, L.P. Goss, W.M. Rocquemore, R.P. Bradley, P.W. Schreiber, and W.B. Roh, Appl. Opt., 18, 2343 (1979).

44. I.A. Stenhouse, D.R. Williams, J.B. Cole, and M.D. Swords, Appl. Opt., 18, 3819 (1979).

45. A.C. Eckbreth, Comb. Flame, 39, 133 (1980).

TABLE 1. Average values and standard deviations for premixed flames on a porous plug burner.

PREMIXED STOICHIOMETRIC H_2-AIR FLAME (ϕ = 1.0)

	Experimental					Theoretical				
	T	$X(N_2)$	$X(H_2O)$	$X(H_2)$	$X(O_2)$	T	$X(N_2)$	$X(H_2O)$	$X(H_2)$	$X(O_2)$
AVE	1773	65.3	33.9	0.1	0.6	1813*	65.1	34.9	0.0	0.0
SD	70	2.2	2.3	0.3	0.3					
RSD	0.04	0.04	0.08							

PREMIXED LEAN H_2 -AIR FLAME (ϕ = 0.55)

	Experimental					Theoretical				
	T	$X(N_2)$	$X(H_2O)$	$X(H_2)$	$X(O_2)$	T	$X(N_2)$	$X(H_2O)$	$X(H_2)$	$X(O_2)$
AVE	1567	69.6	21.1	0.0	9.3	1553*	70.6	20.8	0.0	8.5
SD	62	2.3	1.6	0.1	1.2					
RSD	0.04	0.04	0.09		0.15					

*Measured by radiation corrected thermocouples and cw vibrational Raman bandshape analyses.

TABLE 2. Average values, standard deviations, and normalized moments for turbulent diffusion flames.

TURBULENT H_2-AIR FLAME (Re = 1500)

	Centerline X/D = 50, Y/D = 0					Mixing Layer X/D = 50, Y/D = 3.75				
	T	$X(N_2)$	$X(H_2O)$	$X(H_2)$	$X(O_2)$	T	$X(N_2)$	$X(H_2O)$	$X(H_2)$	$X(O_2)$
AVE	1410	36.5	18.1	43.4	2.0	1844	70.2	18.0	0.7	11.1
SD	162	4.4	2.4	7.6	0.6	250	3.8	4.9	1.4	3.9
RSD	0.11	0.12	0.13	0.17	0.32	0.14	0.05	0.27	2.03	0.35
Z_1	1.00	1.00	1.00	1.00		1.00	1.00	1.00		1.00
Z_2	1.01	1.01	1.02	1.03		1.02	1.00	1.07		1.13
Z_3	1.04	1.04	1.05	1.09		1.05	1.01	1.24		1.37
Z_4	1.08	1.09	1.11	1.19		1.11	1.02	1.55		1.77

TURBULENT H_2-AIR FLAME (Re = 4500)

	Centerline X/D = 50, Y/D = 0					Mixing Layer X/D = 50, Y/D = 5				
	T	$X(N_2)$	$X(H_2O)$	$X(H_2)$	$X(O_2)$	T	$X(N_2)$	$X(H_2O)$	$X(H_2)$	$X(O_2)$
AVE	1484	32.3	18.2	47.6	1.9	1137	73.2	10.2	1.0	15.6
SD	175	4.4	3.2	8.9	0.9	654	16.6	9.5	3.7	8.4
RSD	0.12	0.14	0.18	0.19	0.47	0.58	0.23	0.93	3.70	0.54
Z_1	1.00	1.00	1.00	1.00		1.00	1.00	1.00		1.00
Z_2	1.01	1.02	1.03	1.04		1.33	1.04	1.74		1.25
Z_3	1.04	1.06	1.09	1.10		2.05	1.14	3.54		1.74
Z_4	1.09	1.11	1.20	1.21		3.38	1.30	7.80		2.58

Table 3. Summary of Raman Results for a Laminar Premixed Flame, and at the Centerline and Mixing Layer of Two Turbulent Diffusion Flames.

	LAMINAR PREMIXED FLAME $\phi = 1$	TURBULENT DIFFUSION FLAME Re = 1500 x/d = 50, y/d = 3.75	TURBULENT DIFFUSION FLAME Re = 4500 x/d = 50, y/d = 5.0
AVE	1773.	1844.	1137.
SD	70.	250.	654.
RSD	0.04	0.14	0.58
Z_1	1.00	1.00	1.00
Z_2	1.00	1.02	1.33
Z_3	1.00	1.05	2.05
Z_4	1.01	1.11	3.38

$$Z_L = (\bar{x})^{-L} (J)^{-1} \sum_{j=1}^{J} (x_j)^L$$

Table 4. Raman Data for Turbulent Propane/Hydrogen-Air Flame Shown at the Bottom of Figure 13

Position							
No.	x/d	y/d	Description	T	$X(N_2)$	$X(H_2O)$	$X(H_2)$
1.	25	0	Centerline; Midway between fuel tube tip & bright luminous zone	976 ± 83	0.18 ± 0.03	0.10 ± 0.01	0.63 ± 0.04
2.	50	+4	3/4 way to bright luminous zone from tip, at top edge	1316 ± 82	0.62 ± 0.05	0.12 ± 0.02	0
3.	50	+2	Same, between centerline and top edge	1405 ± 787	0.47 ± 0.14	0.17 ± 0.09	0.01 ± 0.01
4.	50	0	Same, on centerline	All overflows			
5.	75	0	Centerline, in middle of bright luminous zone	All overflows			
6	100	+2.2	Beyond bright luminous zone, at top edge	1842 ± 107	0.53 ± 0.05	0.16 ± 0.03	0
7.	100	0	Same, on centerline	All overflows			

Table 5. Comparison of Raman Scattering and CARS For Turbulent Laboratory Flames

	Raman[a]	CARS[b]
Spatial Resolution	<0.1 mm^3	same
Temporal Resolution	2 μs	10 ns
Repetition Rate	1 pps	10 pps
Temperature		
Accuracy of 100 pulse ave.	about 50K	about 25-50K
Precision of single pulse datum	σ=±4%	±2-7%
Major Species Concentration		
Accuracy of 100 pulse ave.	about 0.01 mole fraction	about 0.03
Precision of single pulse datum	$\sigma \geq \pm 4\%$	±5-10%
Lower conc. limit for single pulse	0.01 mole fraction	0.001-0.02
Simultaneous multi-component measurements	Yes (H_2,N_2,O_2,H_2O)	Difficult

a Based upon GE measurements on laboratory flames.

b Best estimated values from major laboratories (United Technologies Research Center, ONERA, Sandia-Livermore, Systems Research Labs, Harwell, Yale Univ., and others).

Table 6. Range of Applicability for Turbulent Combustion Measurements

	Raman	CARS
H_2 and Nonsooting Hydrocarbon Flames	Yes	Yes
Best Choice for H_2 and Nonsooting Hydrocarbon Flames	X	
Sooting and Spray Flames	Very Limited	Yes (Especially Good for Temp.)
Large Scale Combustors	Very Limited	Wide Applicability
Best Choice for Sooting, Spray Flames, or Large Scale Combustors		X

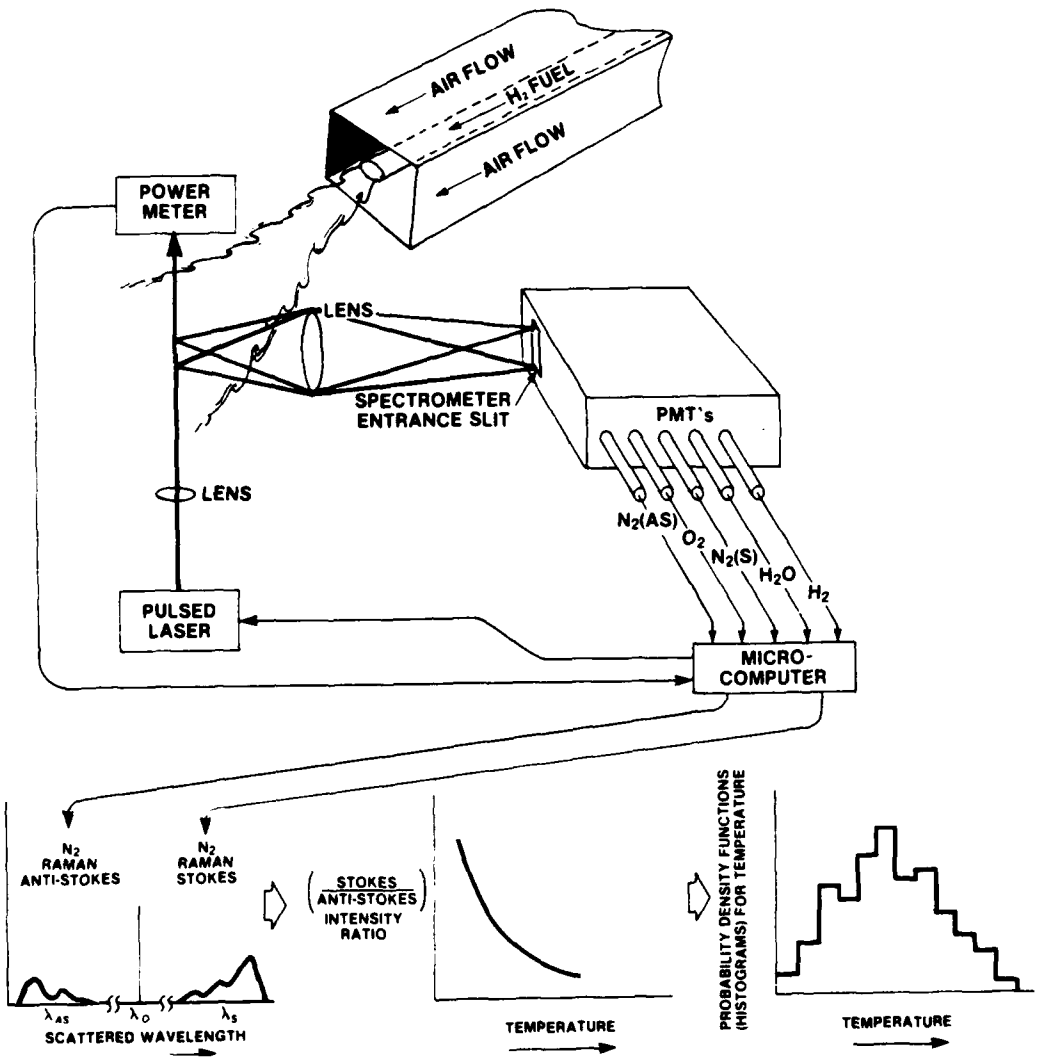

Figure 1. Schematic of Turbulent Combustor Geometry and Optical Data Acquisition System for Vibrational Raman Scattering Measurements of Temperature and Concentrations of Major Flame Species. Also shown are sketches of expected Raman contours of Stokes and anti-Stokes Raman scattering from N_2, the temperature calibration curve, and an example of a probability density function for temperature at a specific location in the flame.

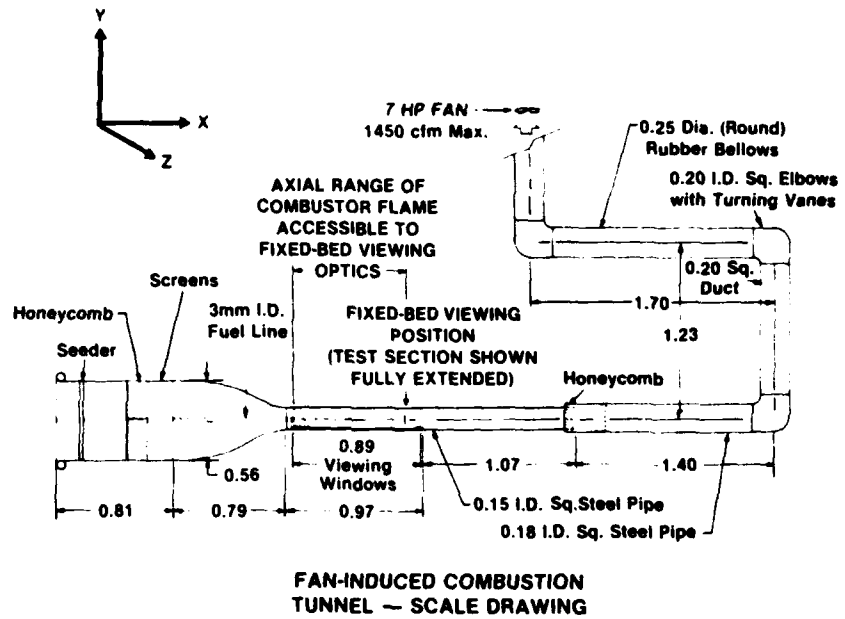

Figure 2a. Scale Drawing of Fan-Induced Combustion Tunnel.

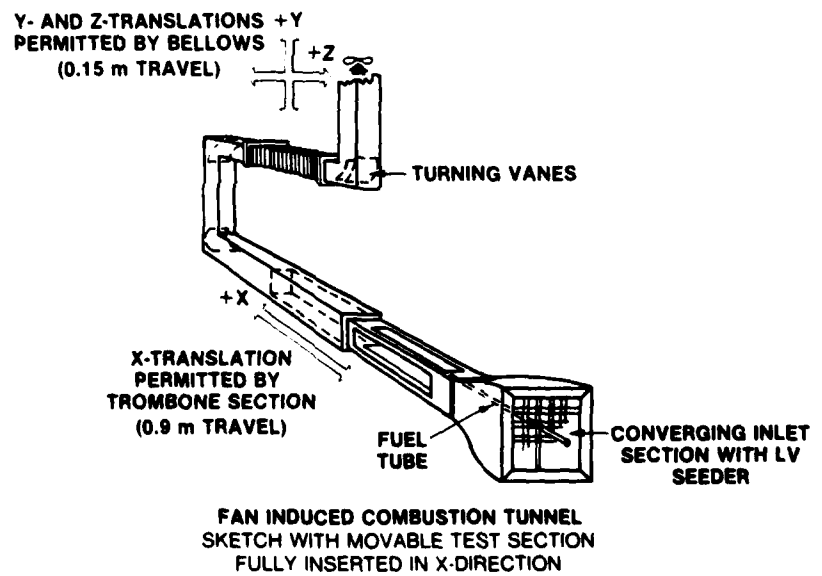

Figure 2b. Isometric Schematic of Fan-Induced Combustion Tunnel, Illustrating Three-Dimensional Translational Capability.

Figure 3. (Top) - View of combustor through window on near side, with fuel tube at left-hand-edge. A hot-film anemometer and a pitot tube are suspended into the flow from a metal plate which replaced the far-side window. (Bottom) - View of combustor from side opposite to that shown in top view. Here, the metal plate replacing the viewing window is instrumented with the pressure taps used to determine the axial pressure gradient.

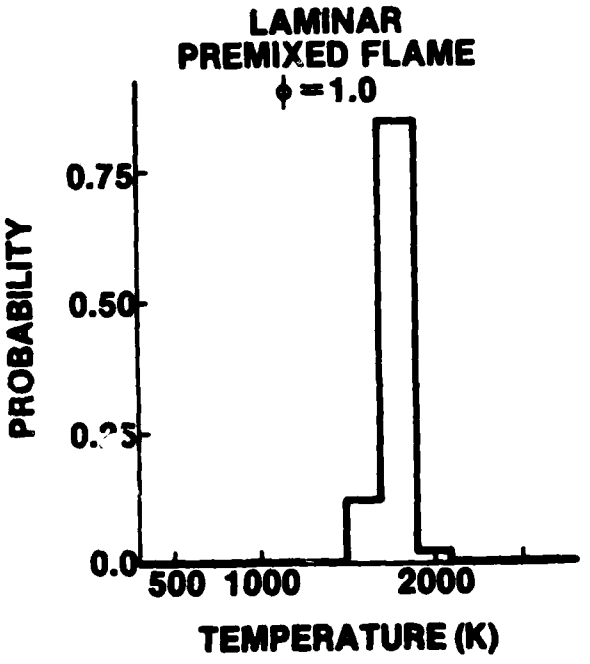

Figure 4. Probability Density Function (Histogram) of Temperature Experimentally Measured in an Isothermal Zone of a Premixed, Laminar H_2-Air Flame with a Fuel-to-Air Equivalence Ratio of 1.0[1]

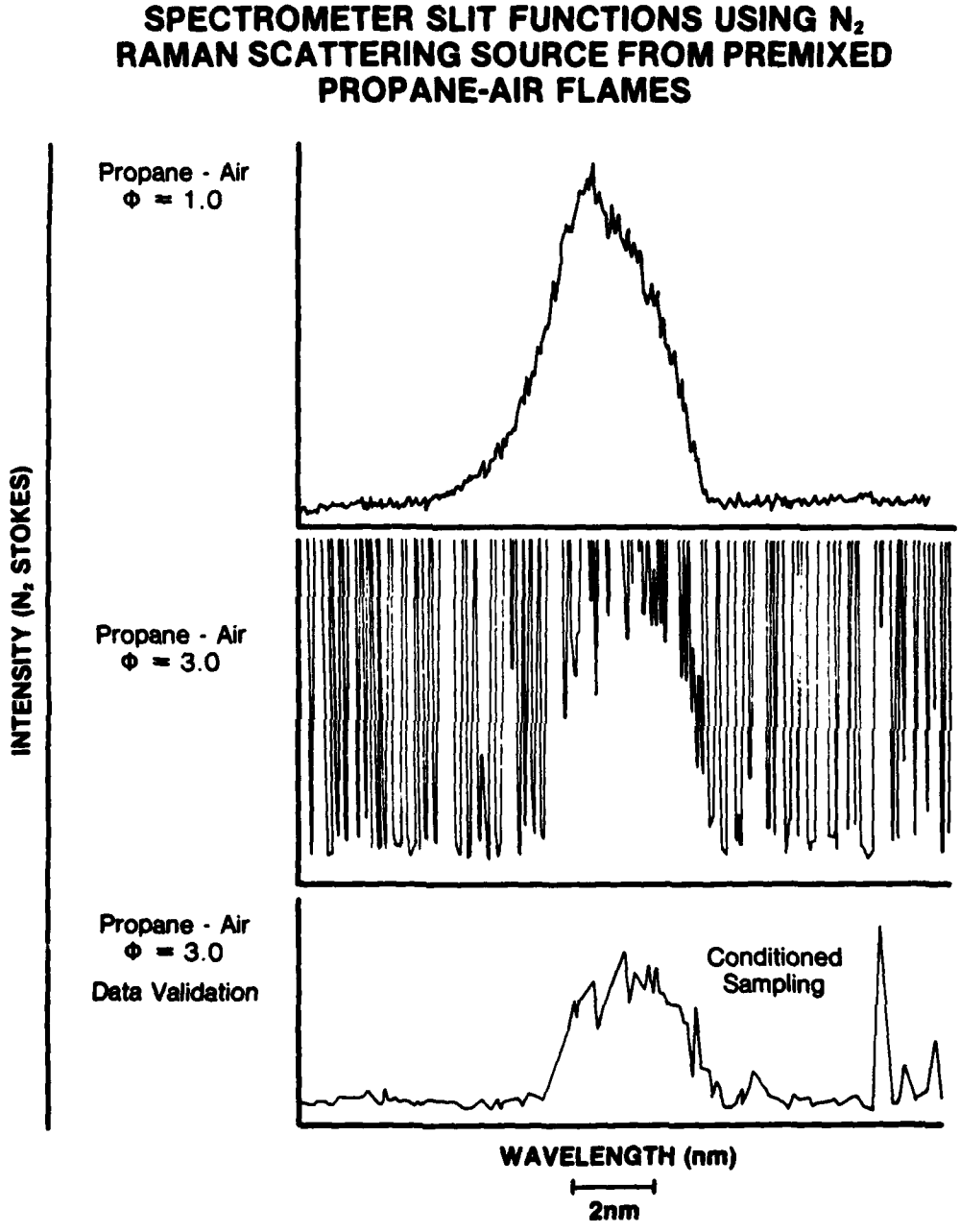

Figure 5. Measurement of Spectrometer Slit Function for Propane-Air Flames Corresponding to Fuel/Air Equivalence Ratios ϕ of 1 and 3.[4,5] For the middle curve, the spikes resulted from strong laser-induced optical signals. The bottom curve has been treated by conditioned sampling. The spike at the right-hand edge is a laser-induced signal that was not suppressed by the sampling threshold.

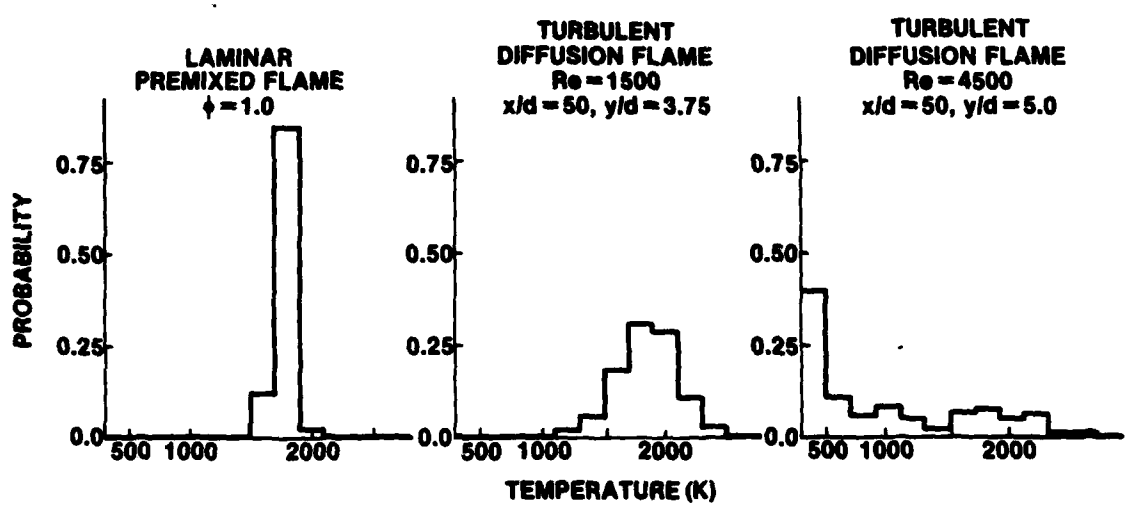

Figure 6. Probability Density Functions (Histograms) of Temperature Experimentally Measured in (a, left) an Isothermal Zone of a Premixed, Laminar H_2-Air Flame with a Fuel-to-Air Equivalence Ratio of 1.0; (b, center) the Mixing Layer of a Moderately Turbulent H_2-Air Jet Diffusion Flame; and (c, right) the Mixing Layer of a More Turbulent H_2-Air Jet Diffusion Flame.[1]

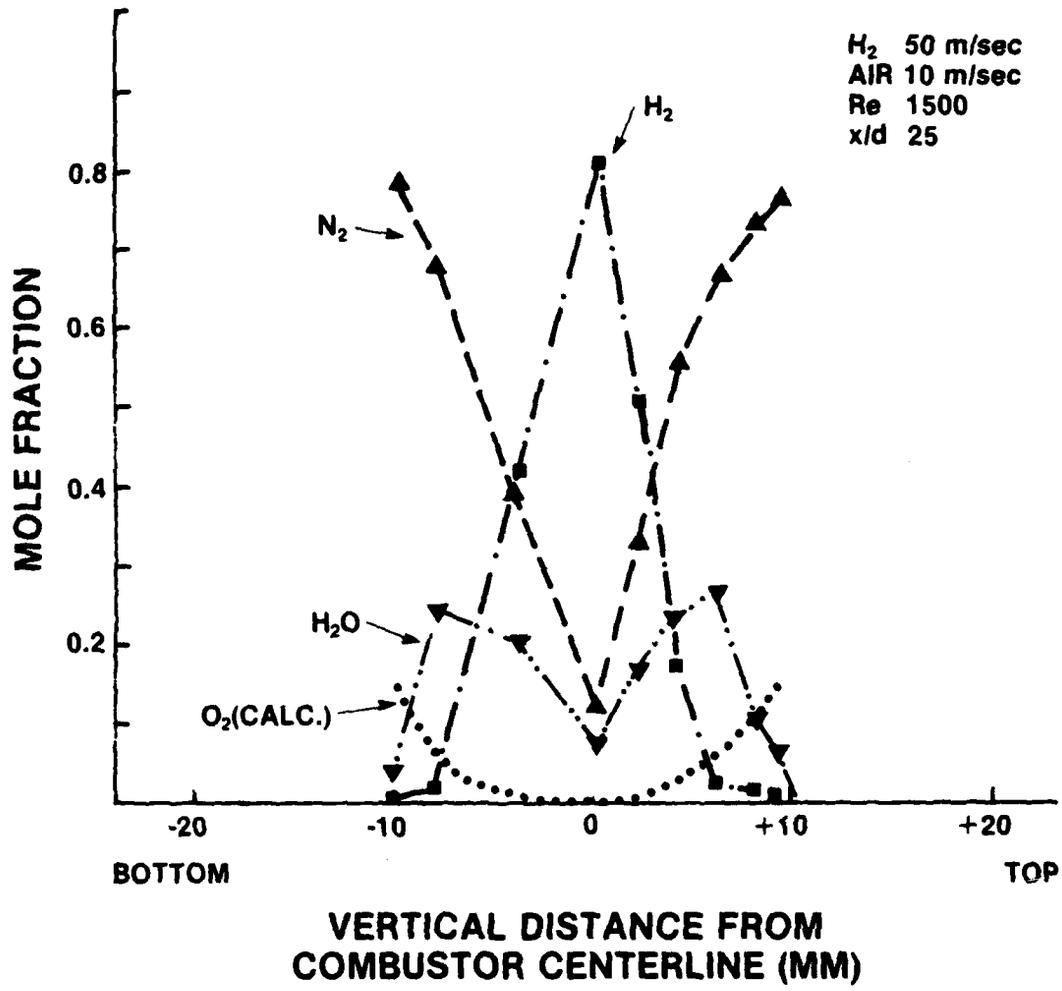

Figure 7. Radial Profiles of Average Values of Major Flame Species Mole Fractions at an Axial Location of 25 Fuel-Tip-Diameters Downstream in a Turbulent H_2-Air Diffusion Flame with a Reynolds Number of 1500.[1] Each data point consists of an average of 200 instantaneous measurements (laser shots). The concentrations of O_2 were not measured here but were calculated assuming a constant ratio of oxygen to nitrogen atoms at all flame locations.

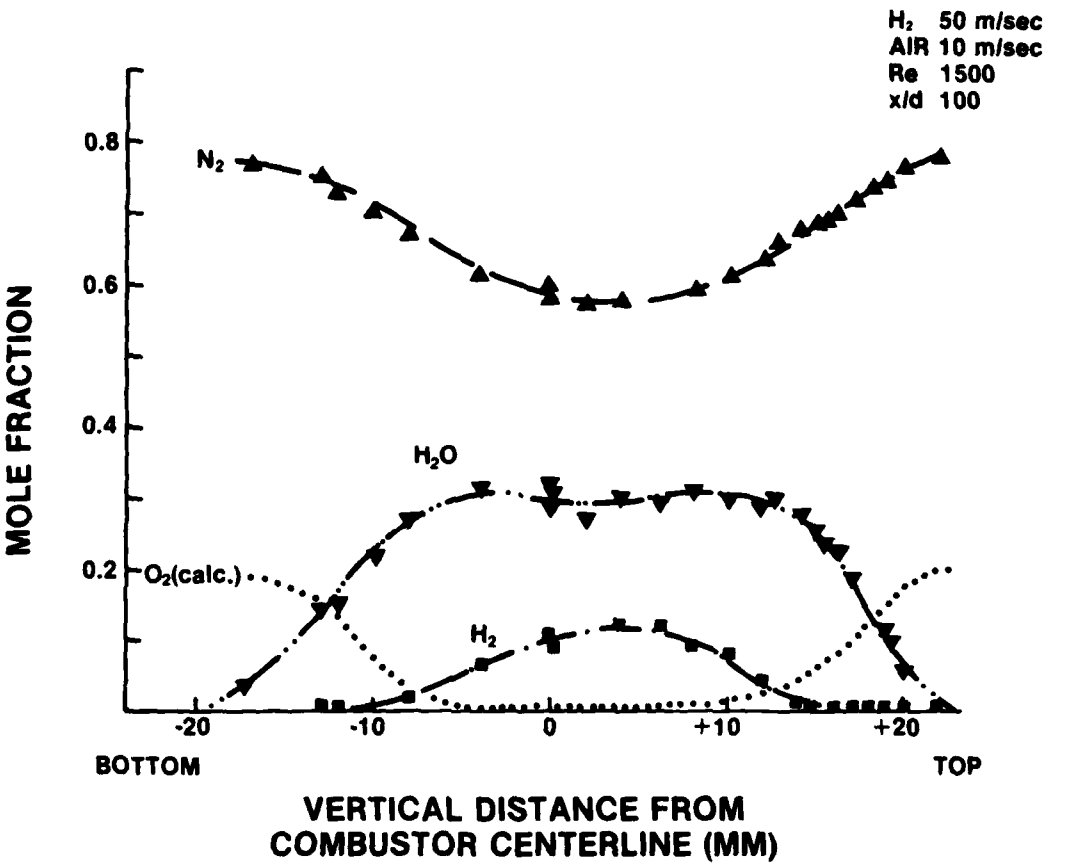

Figure 8. The Same as in Figure 7 Except Further Downstream at an Axial Location of 100 Fuel-Tip-Diamters.[1]

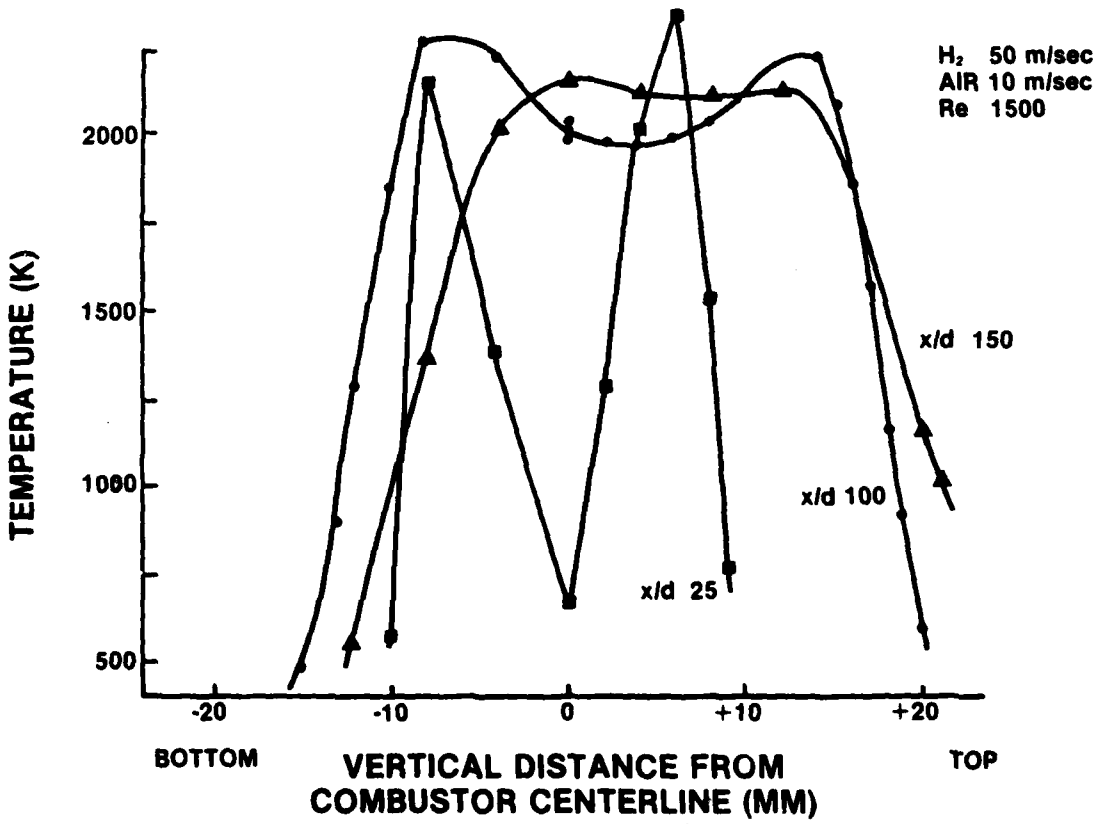

Figure 9. Radial Profiles of Average Values of Temperature at Three Different Axial Locations in a Turbulent H_2-Air Diffusion Flame With a Reynolds Number of 1500.[1] Each data point consists of an average of 200 instantaneous measurements (laser shots).

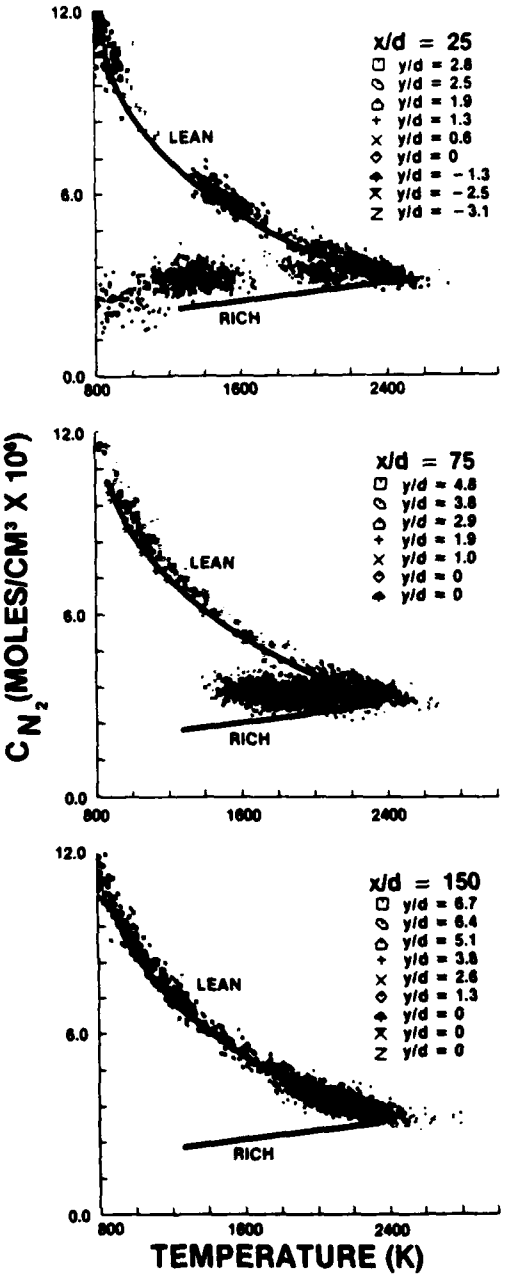

Figure 10. Comparison of Simultaneously Acquired N_2 Concentration and Temperature Data and Adiabatic Equilibrium Model Predictions. These data were taken in the Re = 1500 flame at the various axial and radial positions indicated in the figure.[4]

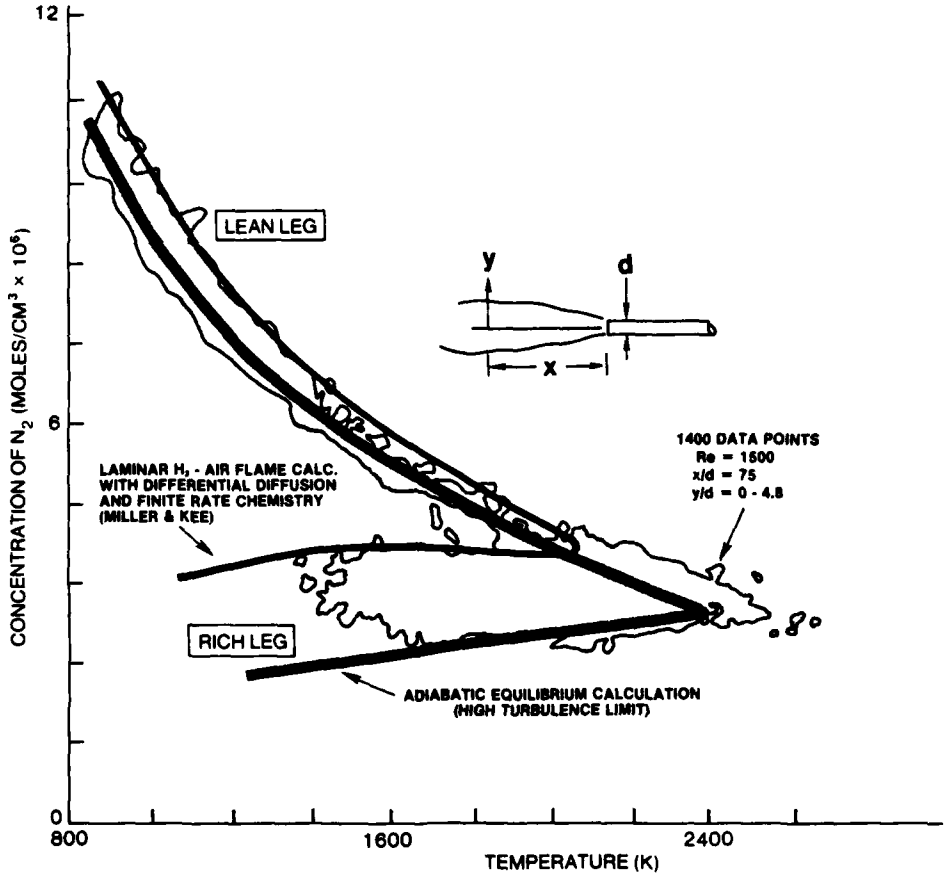

Figure 11. Comparison of Simultaneous Nitrogen Concentration and Temperature Measurements with Laminar (Miller and Kee[8]) and Adiabatic Equilibrium Model Predictions.

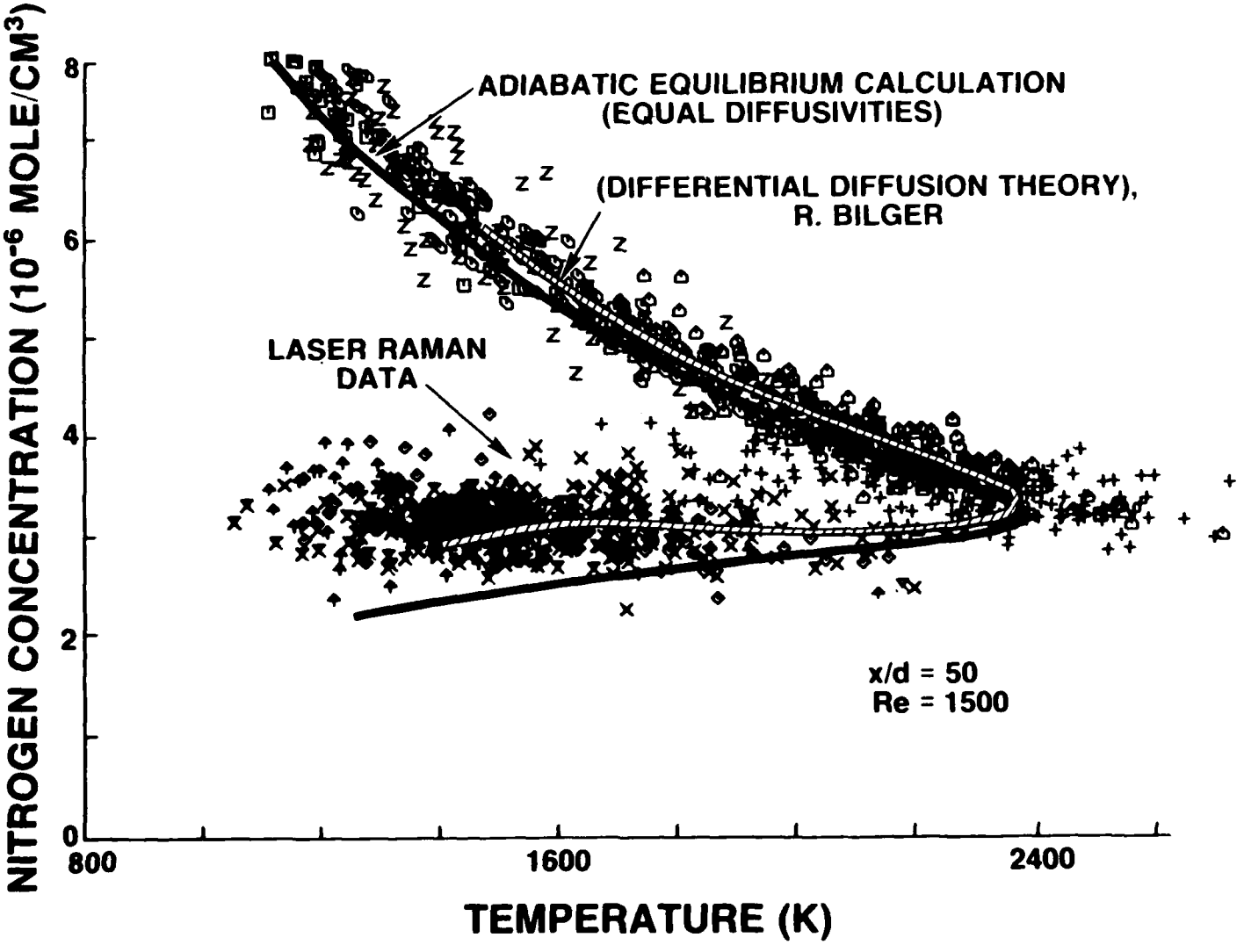

Figure 12. Comparison of Simultaneously Acquired N_2 Concentration and Temperature Data Obtained from a Variety of Radial Positions at an Axial Location 50 Fuel-Tip-Diameters Downstream, with an Adiabatic Equilibrium Calculation Assuming Equal Diffusivities (solid line), and with Mean Values from a Differential Diffusion Calculation by R.W. Bilger (dashed line).[4]

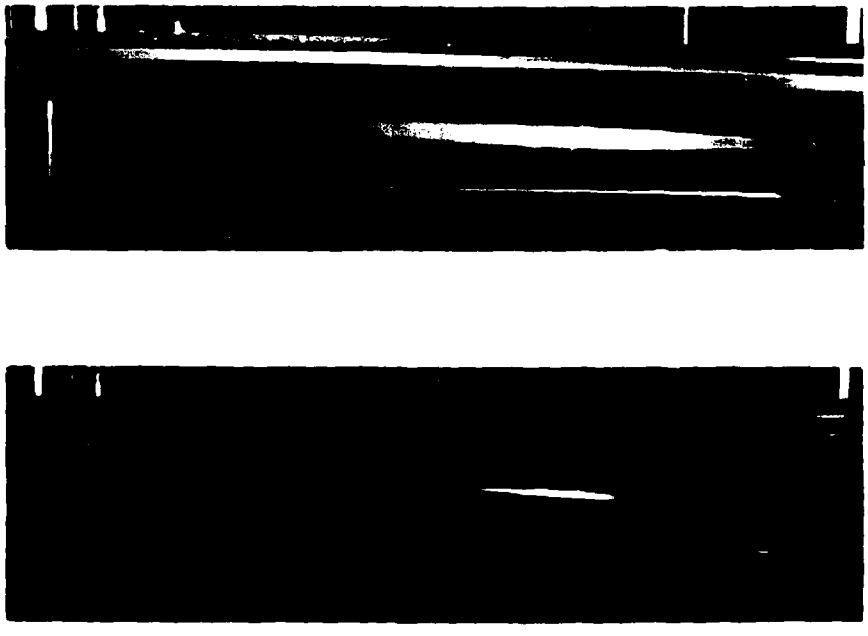

Figure 13. Comparative photographs of H_2-air (top) and propane/H_2 - air (bottom) turbulent diffusion flames. The 3.2-mm-ID fuel tip is visible at the right-hand edge of each picture.

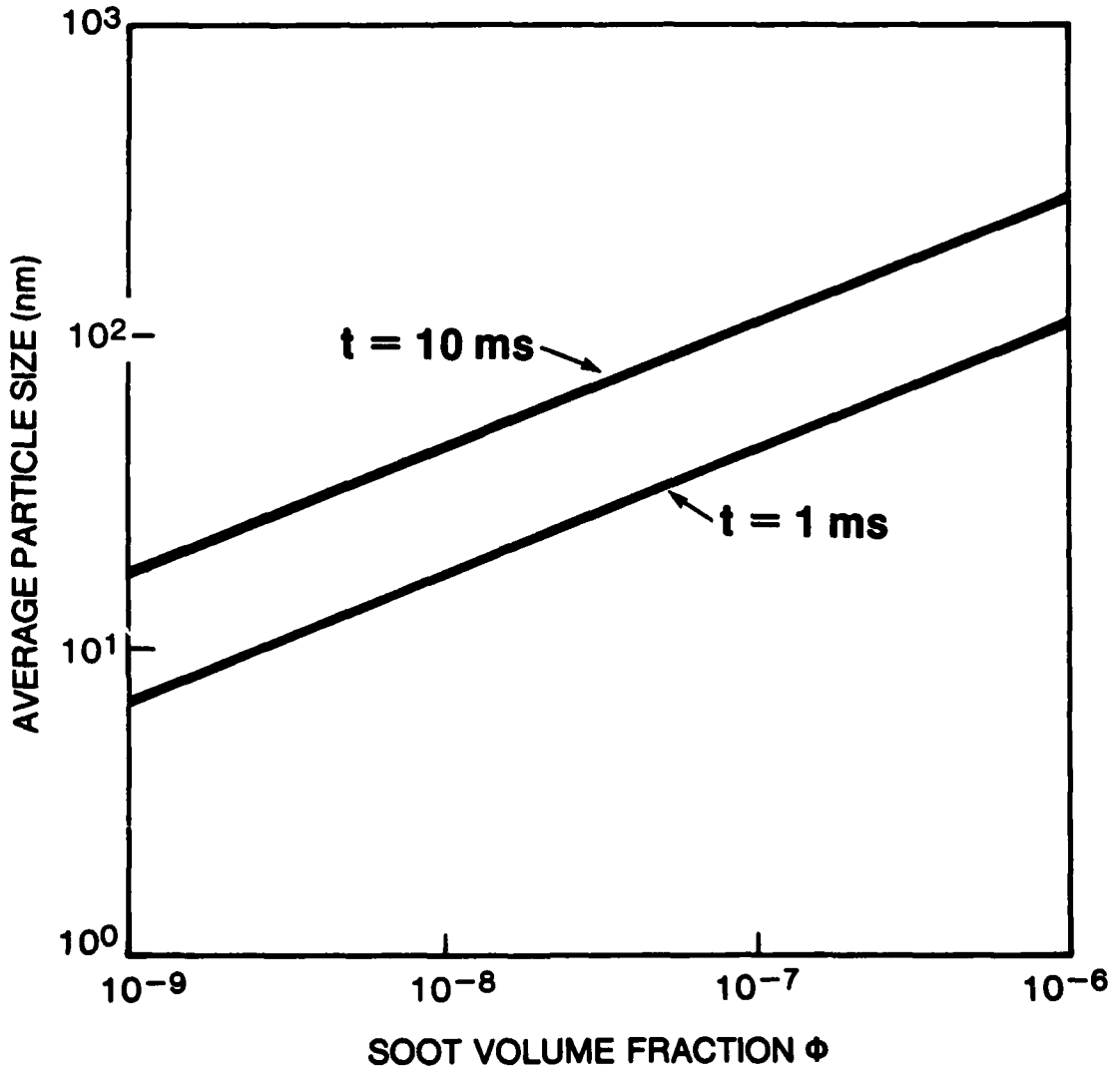

Figure 14. Volume Average Soot Particle Equivalent Radius Calculated From Coagulation Theory, Assuming Soot Created as Fine Particles at Volume Fraction ϕ at Time t Previous to Plot, and Average Size Changes From Coagulation Alone.

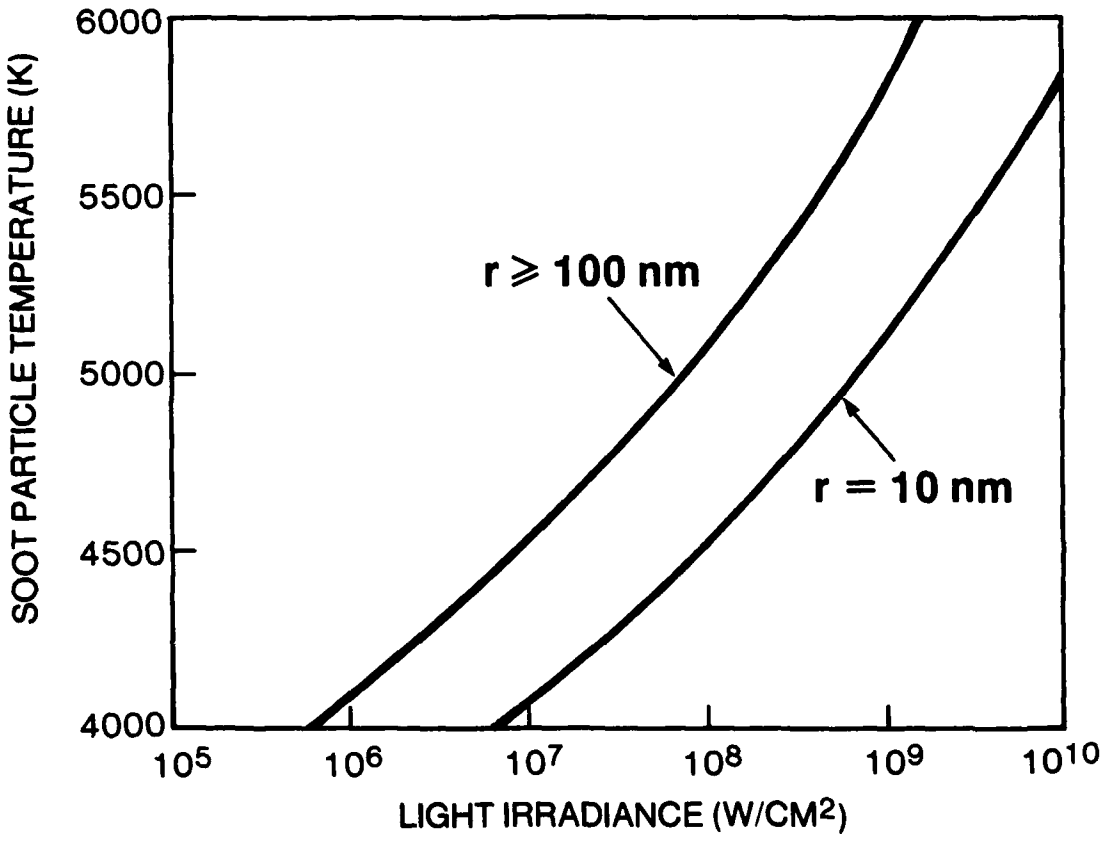

Figure 15. Vaporization-Cooled Soot Particle Temperature as a Function of Laser Beam Irradiance and Particle Radius r.

BIBLIOGRAPHY RELATED TO THIS RESEARCH EFFORT

1. M.C. Drake, M. Lapp, C.M. Penney, S. Warshaw, and B.W. Gerhold, "Measurements of Temperature and Concentration Fluctuations in Turbulent Diffusion Flames Using Pulsed Raman Spectroscopy," Eighteenth Symp. (Int.) on Combustion, The Combustion Institute, 1981, p. 1521.

2. M.C. Drake, M. Lapp, C.M. Penney, S. Warshaw, and B.W. Gerhold, AIAA Paper No. 81-0103 (1981).

3. M. Lapp and R.M.C. So, "The Study of Turbulent Diffusion Flames: Modeling Needs and Experimental Light Scattering Capabilities," AGARD Conference Proceedings No. 281 on Testing and Measurement Techniques in Heat Transfer and Combustion, 1980, Chapt. 19.

4. M. Drake, M. Lapp, C.M. Penney, and S. Warshaw, "Characterization of Turbulent Flames by Single-Pulse Raman Measurements," in Proceedings of the 7th International Conference on Raman Spectroscopy, W.F. Murphy, Ed., North-Holland Publishing Co., Amsterdam, 1980, p. 230.

5. M. Lapp, "Raman Scattering Measurements of Combustion Properties," in Laser Probes for Combustion Chemistry, American Chemical Society Symposium Series, Vol. 134, D.R. Crosley, Ed., American Chemical Society, Washington, D.C., 1980, Chapt. 17.

6. S. Warshaw, M. Lapp, C.M. Penney, and M.C. Drake "Temperature-Velocity Correlation Measurements for Turbulent Diffusion Flames from Vibrational Raman Scattering Data," in Laser Probes for Combustion Chemistry, American Chemical Society Symposium Series, Vol. 134, D.R. Crosley, Ed., American Chemical Society, Washington, D.C., 1980, Chapt. 19.

7. M. Lapp, C.M. Penney, S. Warshaw, and M.C. Drake, "Unlocking the Secrets of Combustion," Industrial Research/Development 21, 116 (1979).

8. M. Lapp, "The Study of Flames by Raman Spectroscopy," in Proceedings of the Sixth International Conference on Raman Spectroscopy, Vol. 1, E.D. Schmid, R.S. Krishnan, W. Kiefer, and H.W. Schrotter, Eds., Heyden and Son Ltd., London, 1978, p. 219.

9. M. Lapp and C.M. Penney, "Instantaneous Measurements of Flame Temperature and Density by Laser Raman Scattering," in Proceedings of the Dynamic Flow Conference 1978 on Dynamic Measurements in Unsteady Flows, Proceedings of the Dynamic Flow Conference, P.O. Box 121, DK-2740 Skovlunde, Demark, 1979, p. 665.